IEEE Open Journal of Signal Processing

Received 23 August 2023; revised 6 January 2024; accepted 16 January 2024. Date of publication 29 January 2024; date of current version 28 February 2024. The review of this article was arranged by Associate Editor Fan Liu.

Digital Object Identifier 10.1109/OJSP.2024.3359997

Optimum Waveform Selection for Target State Estimation in the Joint Radar-Communication System

ASHOKA CHAKRAVARTHI MAHIPATHI [1] (Member, IEEE), BETHI PARDHASARADHI [1] (Member, IEEE), SRINATH GUNNERY [1] (Member, IEEE), PATHIPATI SRIHARI [1] (Senior Member, IEEE), JOHN D'SOUZA [1] (Member, IEEE), AND PARAMANANDA JENA [2] (Member, IEEE)

[1]Department of ECE, National Institute of Technology Karnataka, Surathkal 575025, India
[2]Electronics and Radar Development Establishment (LRDE), DRDO, Bangalore 560093, India

CORRESPONDING AUTHOR: PATHIPATI SRIHARI (e-mail: srihari@nitk.edu.in).

This work was supported by the Cumulative Professional Development Allowance (CPDA) granted to John DSouza by the Ministry of Education, Government of India.

ABSTRACT The widespread usage of the Radio Frequency (RF) spectrum for wireless and mobile communication systems generated a significant spectrum scarcity. The Joint Radar-Communication System (JRCS) provides a framework to simultaneously utilize the allocated radar spectrum for sensing and communication purposes. Generally, a Successive Interference Cancellation (SIC) based receiver is applied to mitigate mutual interference in the JRCS configuration. However, this SIC receiver model introduces a communication residual component. In response to this issue, the article presents a novel measurement model based on communication residual components for various radar waveforms. The radar system's performance within the JRCS framework is then evaluated using the Fisher Information Matrix (FIM). The radar waveforms considered in this investigation are rectangular pulse, triangular pulse, Gaussian pulse, Linear Frequency Modulated (LFM) pulse, LFM-Gaussian pulse, and Non-Linear Frequency Modulated (NLFM) pulse. After that, the Kalman filter is deployed to estimate the target kinematics (range and range rate) of a single linearly moving target for different waveforms. Additionally, range and range rate estimation errors are quantified using the Root Mean Square Error (RMSE) metric. Furthermore, the Posterior Cramer-Rao Lower Bound (PCRLB) is derived to validate the estimation accuracy of various waveforms. The simulation results show that the range and range rate estimation errors are within the PCRLB limit at all time instants for all the designated waveforms. The results further reveal that the NLFM pulse waveform provides improved range and range rate error performance compared to all other waveforms.

INDEX TERMS Fisher information matrix, Joint radar-communication system, Measurement noise covariance, PCRLB, RMSE, Target tracking.

I. INTRODUCTION

The radio spectrum is highly congested due to the proliferation of the telecommunication sector and the abundant RF users. Researchers are looking to reuse the RF spectrum, currently allocated to various societal applications, to overcome this problem. The radar spectrum is the finest choice to be accessed and shared owing to the considerable amount of RF spectrum accessible at the radar sensor frequency band [1]. Primarily, the significance of co-existence and spectrum sharing among radar sensor and communication systems was elucidated in [2]. Further, the co-existence of a radar sensor and communication systems was presented in [3]. Furthermore, the performance of the spectrum-sharing radar in a multipath environment was analyzed in [4]. Radar and communication system spectrum-sharing approaches are broadly categorized into spectral co-existence and cooperation. In the spectral co-existence scheme, mutual interference is the vital issue [5]. A spectral cooperation scheme was introduced in [6] to suppress mutual interference. In the spectral cooperation approach, the information about the channel condition is

exchanged among the radar sensor and communication system to improve the performance of both subsystems. Besides that, an elaborated review on radar sensors and communication spectrum sharing is provided in [7].

The crucial step in developing the Joint Radar-Communication System (JRCS) is to identify a suitable waveform applicable for sensing and communication system purposes [8]. Being radar is the primary user, and it is inevitable to maintain the radar system performance, specifically for defense applications. To achieve that, the design of a radar waveform for JRCS plays a significant role in developing advanced radar sensor systems [9]. Especially in a radar sensor, the choice of transmitted waveform and its tunable parameters plays a crucial role in the target tracking performance [10]. In [11], researchers initiated the design of waveforms for a JRCS by broadcasting communication data using pulse interval-modulated radar pulses. Furthermore, [12] explored a radar waveform that serves both sensing and communicative functions within a JRCS environment. In contrast to the previous approach, [13] selects two distinct waveforms for communication and radar systems. Nevertheless, the performance enhancement of a JRCS in the aforementioned approach heavily relies on waveform constraints, as discussed in [14]. Another communication, [15], introduced a radar-centric method where optimizing the radar waveform enhances the performance of a coexisting radar-communication system. On the other hand, in the communication-centric approach [16], the communication waveform is optimized to improve the performance of a JRCS. Furthermore, researchers in [17] design an optimal radar waveform using the Cramer-Rao Lower Bound (CRLB) to estimate target parameters within a JRCS framework. Later, the effect of communication interference on the dynamic threshold detector at the joint radar-communication receiver is investigated in [18]. Recently, researchers in [19] studied the coherent detection of radar returns in the presence of in-band interference from cyclostationary modulated communication signals.

Target tracking is an important aspect of a radar-sensing system to estimate the trajectory of a radar target within a surveillance space. The major blocks present in the target tracking system are track-filtering and data association. Track-filtering involves determining the target trajectory (i.e., target position, target velocity) of a track using sensor measurements (i.e., target range, azimuth angle, and elevation angle) that are assigned to the track [20]. Data association is the process of associating the measurement to a particular track [20]. The Kalman Filter (KF) predicts the target state at the instant of the most recent radar measurement based on the present target state. It gives an optimal state estimate subject to linearity and Gaussian distribution [21]. Subsequently, researchers considered various types of Kalman Filters, such as extended, unscented, and particle filters, to address the challenge posed by non-linearity [22]. In the context of data association, traditional association approaches like Nearest Neighbour (NN) and Global Nearest Neighbour (GNN) are used to extract a unique measurement out of all accessible measurements present in the validation gate [23]. Alternatively, [24] presents a Probabilistic Data Association (PDA) approach to guarantee a linear combination of all radar measurements within the validation gate. Regarding tracking management, [25] outlines two general approaches: quality-based track maintenance and logic-based track maintenance.

The traditional method of designing the target tracking system considers the sensor and tracking sub-systems as entirely separate entities [26]. Authors in [27] accomplished significant performance enhancement for a tracking system by integrating the waveform optimization block (sensor) into a target tracking system. Further, researchers have demonstrated that adaptive waveform design schemes significantly enhance the performance of the target tracking system [9]. Furthermore, researchers assess information about the target environment based on previous measurements and utilize it to modify the waveform for subsequent signal transmission, achieving optimal tracking performance [28]. In [9], researchers initially introduced adaptive waveform selection for radar target tracking, identifying tunable waveform specifications for tracking in a unidirectional clutter-free environment. Later, they presented adaptive waveform selection schemes in [27] to improve target tracking performance in a cluttered environment. Furthermore, the researchers analyzed the adaptive waveform selection schemes to enhance target tracking performance in a two-dimensional scenario under a wideband environment, as detailed in [29]. The target tracking the performance of various waveforms was analyzed using the statistically estimated steady-state error [30]. In [31], researchers applied a stochastic-approximation-based particle filter to optimize the waveform parameters and reduce the tracking error variance. They presented a benchmark problem in [32] to track moving targets in the presence of Electronic Counter Measurements (ECM) and false alarms. A waveform agile target tracking review was presented in [33]. Further, it also explained the significance of dynamic waveform selection for tracker requirements. In another communication, researchers in [34] present a systematic method based on waveform agile sensing aimed at improving the performance of benchmark target tracking in the presence of hefty interference. Later, researchers improved target estimation performance by exploiting the target returns from a communication transmitter, as documented in [35]. Recently, analysts analyzed radar target tracking performance for in-band communication interference within a joint radar-communication system, as outlined in [36].

The comprehensive literature review above reveals a limited emphasis on reporting optimal waveform selection and track filtering to enhance tracking performance within the JRCS framework. This observation has inspired our current research, investigating optimal waveform design for the JRCS configuration. Target tracking within the JRCS framework, specifically about optimal waveform selection, remains an unexplored area in prior studies. As a result, our research

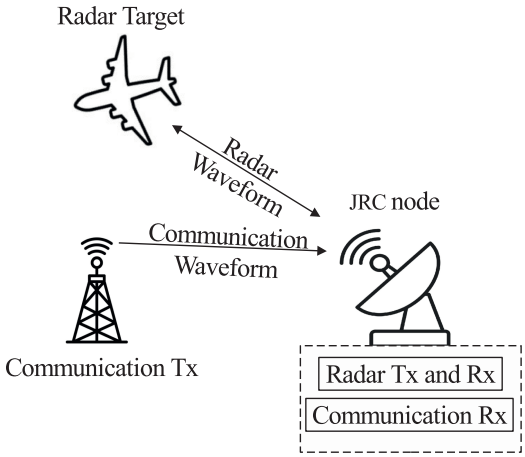

FIGURE 1. Joint radar-communication system model.

is dedicated to evaluating optimal waveform selection in the JRCS configuration, making the following contributions:

- Measurement noise covariance matrix is derived for various waveforms to characterize the sensor behavior in the presence of communication residual component for the Joint Radar-Communication System(JRCS).
- The Kalman Filter (KF) is applied to estimate the trajectory of a linearly moving target with the obtained measurements for different waveforms using the novel measurement model for the JRCS.
- The proposed work conducts the performance validation of a radar sensor for various designated waveforms, namely rectangular pulse, triangular pulse, Gaussian pulse, LFM pulse, LFM-Gaussian pulse, and NLFM pulse by the PCRLB limit.

The remainder of this article is coordinated as follows. Section II describes the working scenario and problem formulation. Section III presents the sensor characterization and evaluation of various waveforms' measurement noise covariance matrix. Further, Section IV explains the motion model, measurement model, and track filtering. Furthermore, the results and analysis are discussed in Section V. Eventually, Section VI wraps up this article with conclusions.

II. PROBLEM FORMULATION

Fig. 1 depicts the Joint Radar-Communication System (JRCS) framework, where the Joint Radar-Communication (JRC) node is capable of detecting the radar target and acting as a communication receiver. The JRC node uses the same spectral band and coverage area for sensing and communication purposes. Further, the radar system can receive communication signal information. Here, the radar is fully synchronized with the communication system to maintain transmission efficiency and to accomplish improved radar sensing within the coverage area [37], [38].

The radar and communication systems generally have distinct waveform requirements [13]. Therefore, the proposed waveform selection approach considered that radar and communication systems use separate waveforms for transmission, and a radar-centric approach [39] is considered in the current scenario. The signal received at the JRC node is provided by,

$$y(t) = s_{rad}(t-\tau) + s_{com}(t) + n(t), \tag{1}$$

where '$s_{rad}(t-\tau)$' represents the radar return, '$s_{com}(t)$' indicates the received communication signal, and '$n(t)$' represents thermal noise present in the receiver. Here,'τ' indicates the round trip time delay and is given by,

$$\tau = \frac{2R}{c}, \tag{2}$$

Here, 'c' denotes the velocity of light, and 'R' represents the target's distance from the radar sensor. Further, we assume that the JRC node employs the successive interference cancellation (SIC) receiver model [6] to combat the mutual interference between radar sensing and communication systems. However, the performance of a SIC receiver model is super sensitive to model-mismatch errors [13]. In addition, they bring in higher residual components, which badly affects the interference-cancellation process. The likely sources for model mismatch errors are phase noise and dynamic range constraints on the receiver. In this article, we concentrated on how phase noise solely influences the performance of a joint radar-communication System. In [40], researchers comprehensively analyze the interconnection between phase noise and the SIC receiver.

In the SIC receiver model, we assume that, based on prior observations, there is awareness of the radar target range. Utilizing this knowledge, the JRC node generates a predicted radar return and suppresses it from the received signal, as outlined in (1). The JRC node decodes the communication symbols once the radar signal is predicted, as documented in [13]. However, due to phase noise, there is a deviation between the received and decoded communication signals, adding a residual component to the radar return. Hence, in the presence of communication residual, the JRC node extracts radar target information from the received signal (1). Therefore, the affected received signal at the JRC node from a radar sensor perspective is provided by,

$$y(t) = s_{rad}(t-\tau) + s_{com}^{resi}(t) + n(t), \tag{3}$$

With reference to [6], the communication residual component ($s_{com}^{resi}(t)$) is expressed as,

$$\begin{aligned} s_{com}^{resi}(t) &= s_{com}(t) - s_{com}^{decoded}(t) \\ &= \frac{\partial s_{com}(t)}{\partial t} n_{\tau,\text{proc}}. \end{aligned} \tag{4}$$

Here, '$s_{com}^{resi}(t) + n(t)$' represents the interference residual plus noise component, '$s_{com}(t)$' represents the received communication signal, '$s_{com}^{decoded}(t)$' represents the decoded communication signal, and '$n_{\tau,\text{proc}}$' represents the process noise having variance ($\sigma^2_{\tau,\text{proc}}$). We assume that noise is an additive white bandpass Gaussian noise with a spectral height '$N_0/2$'. Further, to obtain valid inferences from the residual component, it should follow a Gaussian distribution [41]. Here, we assume the spectral height of the residual communication component as '$N_r/2$'. In addition, in (3), the '$s_{rad}(t-\tau)$' represents the

TABLE 1. Parameters Considered for Evaluating the Measurement Noise Covariance Matrix

Parameter	Value
Operating Bandwidth (B)	5 MHz
Operating frequency at the center (f)	3 GHz
Target range of a radar system (R)	50 km
Antenna gain of a radar (G_r)	40 dBi
Radar transmitted power (P_t)	1 MW
Target cross-section area of a radar (σ_a)	30 m^2
Temperature (T_k)	1000 K
Boltzmann constant (K_B)	1.38x10^{-23} J/K
Overall communication antenna gain and propagation loss (b)	6.33x10^{-13}
Transmitted communication signal power (P_{comm})	300 mW
Power spectral density of phase noise (η_0)	-110 dBc/Hz
Range fluctuation process variance ($\sigma_f{}^2$)	25 m^2
Time-bandwidth product (TB)	128
Range of the communication system	10 km

baseband envelope owing to target return and is provided by

$$s_{rad}(t-\tau) = \sqrt{E_r} e^{j\Phi} \tilde{x}(t-\tau) e^{j v_0 t} \tag{5}$$

Here, 'E_R' represents the energy of the target return, 'Φ' represents the random phase shift, '$\tilde{x}(t)$' represents the transmitted signal envelope, 'v_0' represents the Doppler shift, and 'τ' indicates the target delay. The normalized communication residual spectral density is given by [13],

$$N_r(f) = \left(4\pi^2\right) \|b\|^2 P_{comm}\, \eta_0 {\sigma_f}^2 \|S_{com}(f)\|^2 f^2. \tag{6}$$

Here 'b' represents overall communication antenna gain and propagation loss, 'P_{comm}' represents the transmitted communication signal power, 'η_0' represents the phase noise spectral density, 'σ_f' represents the process noise variance, '$S_{com}(f)$' represents the spectrum of received communication signal component, and 'f' is the frequency. According to the frequency range of operation, the Quadrature Amplitude Modulated (QAM) signal is widely preferred for transferring communication data in a joint radar-communication scenario [1]. However, the specifications related to the QAM communication signal are presented in Table 1. Subsequently, the thermal noise spectral density is expressed as,

$$N_0(f) = K_B T_K \Pi_B(f) \tag{7}$$

Here, 'K_B' represents the Boltzmann constant, 'T_K' represents temperature in Kelvin degree and '$\Pi_B(f)$' represents the rectangular spectrum. Based on above equations (6) and (7), thermal noise power (N_0), and communication residual noise power (N_r) are evaluated.

The radar sensor should process the signal during the intra-pulse time slot of the received pulse [9]. Generally, the sensor estimates the target state and velocity. The radar tracker needs to process information during the inter-pulse time slot of the received pulse, as indicated in [9]. Of course, there is an indirect connection between radar sensor measurement and tracking. However, the quality of a radar sensor measurement mainly depends on waveform selection. Thus, optimal waveform selection plays a vital role in improving tracking performance. In this regard, in our work, firstly, we derived the measurement noise covariance matrix ($\mathbf{N}(\mathbf{\Theta_k})$) for various waveforms to test the quality of measurement. Further, we applied the Kalman filter to obtain a single target track using these measurements with RMSE as a metric to accomplish enhanced radar target tracking performance for both range and range rate.

The foundation of the proposed target tracking framework rests upon the previous significant work presented in [9] and [27]. From Fig. 2(a), the tracking filter aims to estimate the target state from a set of noisy measurements [9]. It is observed that the radar sensor contains both transmitter, a receiver, and an optimal receiver sub-section for better detector performance. The signal processor performs pulse compression and Doppler processing to improve the range resolution [20]. Subsequently, the optimal detector selects the appropriate threshold level to accomplish the best possible detection probability of a target.

Further, the tracking filter estimates the target position and velocity based on the measurements. In addition, a feedback loop depicted in Fig. 2(a) shows the dependency of target tracking on waveform optimization. Here, the waveform optimization block is considered to have proper control over the radar-transmitted waveform and its parameters [27]. In addition, the measurement quality mainly relies on the waveform selection. Furthermore, it provides information regarding selecting the following transmitted waveform by the tracker requirement. Moreover, Fig. 2(b) depicts the detailed idea of the waveform selection process.

In a nutshell, the proposed target tracking framework addresses the significance of waveform selection for a better target state estimation performance in the JRCS environment. Additionally, we analyze the performance of target state estimation in the presence of a communication residual component.

III. RADAR SENSOR CHARACTERIZATION

The characterization of a radar sensor mainly relies on knowledge of the measurement noise covariance matrix ($\mathbf{N}(\mathbf{\Theta_k})$) [9]. Further, it is a waveform-dependent non-linear function of the waveform parameter vector ($\mathbf{\Theta_k}$). Here, '$\mathbf{\Theta_k}$' provides the information regarding the received waveform parameters of the designated waveform at the time instant '$\mathbf{k}$'. The relation between the waveform parameter vector '$\mathbf{\Theta}_k$' and the covariance matrix of the noisy observations ($\mathbf{N}(\mathbf{\Theta_k})$) is obtained by the measurement noise covariance matrix, as derived in [9]. This relation is expressed as

$$\mathrm{E}\left[(\mathbf{y}-\bar{\mathbf{y}})(\mathbf{y}-\bar{\mathbf{y}})^T\right] = \mathbf{N}(\mathbf{\Theta_k}) = \mathbf{T}\mathbf{J}^{-1}\mathbf{T}^T \tag{8}$$

Here $\mathbf{y} = \mathbf{T}\alpha$, '$\mathbf{y}$' represents the measurement vector of the tracking system, and it is formed based on a range (r)

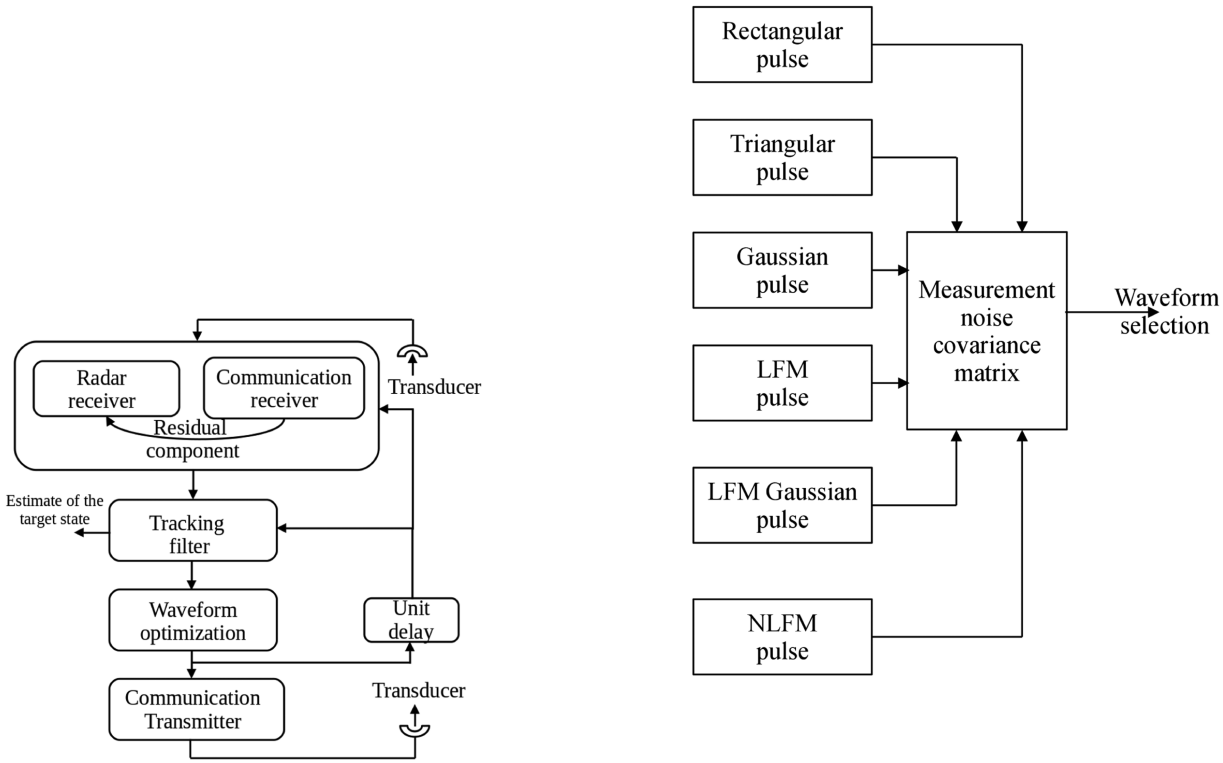

(a) Proposed target tracking framework

(b) Waveform selection strategy

FIGURE 2. Optimal waveform selection for the target tracking scenario.

and range-rate ($\dot{r}$), i.e., $\mathbf{y} = [r\ \dot{r}]^T$. Subsequently, '$\bar{\mathbf{y}}$' represents the mean of the measurement vector '$\mathbf{y}$'. Whereas, '$\boldsymbol{\alpha}$' represents the receiver estimation parameter vector, and it is formed based on the received signal vector, i.e., $\alpha = [\tau\ \omega]^T$. Here '$\tau$' is the time delay, and 'ω' represents the Doppler frequency. Further, '$\mathbf{T}$' is the transformation matrix and it is given by [31], $\mathbf{T} = \text{diag}(c/2, c/(2\omega_c))$. Here '$c$' represents the waveform propagation velocity, and ω_c is the carrier frequency. '$\mathbf{J}$' represents the Fisher information matrix. From (8), it is evident that Fisher's information matrix needs to be evaluated to determine the measurement noise covariance matrix ($\mathbf{N}(\boldsymbol{\Theta}_\mathbf{k})$).

A. CALCULATION OF FISHER INFORMATION MATRIX (J)

In general, the Fisher information matrix is represented as,

$$\begin{bmatrix} J_{11} & J_{12} \\ J_{21} & J_{22} \end{bmatrix} \tag{9}$$

According to the parameters of interest (τ and ω), the Fisher information matrix elements are defined as,

$$J_{11} = -\mathrm{E}\left[\frac{\partial^2}{\partial \tau^2} \ln \Lambda\,(\tau, \omega)\right] \tag{10}$$

$$J_{22} = -\mathrm{E}\left[\frac{\partial^2}{\partial \omega^2} \ln \Lambda\,(\tau, \omega)\right] \tag{11}$$

$$J_{12} = J_{21} = -\mathrm{E}\left[\frac{\partial^2}{\partial \tau \partial \omega} \ln \Lambda\,(\tau, \omega)\right] \tag{12}$$

Firstly, it is necessary to determine the log-likelihood function to obtain the fisher information parameters. According to [42], the log-likelihood function corresponding to the received signal (3) at the JRC node is evaluated as,

$$\ln \Lambda\,(\tau, \omega) = \frac{1}{N_0 + N_r} \frac{\bar{E}_r}{\bar{E}_r + N_0 + N_r} \left\{|L(\tau, \omega)|^2\right\} \tag{13}$$

Here, $\bar{E}_r$ represents the average received signal energy. Subsequently, the likelihood function is expressed as

$$L(\tau, \omega) = \int_{\infty}^{\infty} y(t)\tilde{x}^*(t - \tau) \exp^{-j\omega t}\, dt \tag{14}$$

from (79),

$$\begin{aligned} \frac{\partial \ln \Lambda(\tau, \omega)}{\partial \tau} &= K' \left[L(\tau, \omega)\tfrac{\partial L^*(\tau, \omega)}{\partial \tau} + \tfrac{\partial L(\tau, \omega)}{\partial \tau} L^*(\tau, \omega)\right], \\ &= 2\,K' \mathrm{Re}\left[L(\bar{\tau}, \omega)\frac{\partial L^*(\tau, \omega)}{\partial \tau}\right] \end{aligned} \tag{15}$$

Here,

$$K' \triangleq \frac{1}{N_0 + N_r} \frac{\bar{E}_r}{\bar{E}_r + N_0 + N_r} \tag{16}$$

subsequently, the following derivatives are required to evaluate the elements of the Fisher information matrix (J),

$$\frac{\partial^2 \ln \Lambda(\tau,\omega)}{\partial \tau^2} = 2K'\mathrm{Re}\left[\frac{\partial L(\tau,\omega)}{\partial \tau}\cdot\frac{\partial L^*(\tau,\omega)}{\partial \tau} + L(\tau,\omega)\frac{\partial^2 L^*(\tau,\omega)}{\partial \tau^2}\right] \tag{17}$$

$$\frac{\partial^2 \ln \Lambda(\tau,\omega)}{\partial \tau \partial \omega} = 2K'\mathrm{Re}\left[\frac{\partial L(\tau,\omega)}{\partial \omega}\cdot\frac{\partial L^*(\tau,\omega)}{\partial \tau} + L(\tau,\omega)\frac{\partial^2 L^*(\tau,\omega)}{\partial \tau \partial \omega}\right] \tag{18}$$

$$\frac{\partial^2 \ln \Lambda(\tau,\omega)}{\partial \omega^2} = 2K'\mathrm{Re}\left[\frac{\partial L(\tau,\omega)}{\partial \omega}\frac{\partial L^*(\tau,\omega)}{\partial \omega} + L(\tau,\omega)\frac{\partial^2 L^*(\tau,\omega)}{\partial \omega^2}\right] \tag{19}$$

$$J_{11} = -E\left\{\frac{\partial^2 \ln \Lambda(\tau,\omega)}{\partial \tau^2}\right\} \tag{20}$$

$$= -2K'\left\{\int_{-\infty}^{\infty}\frac{\partial \tilde{x}^*(t-\tau)}{\partial \tau}\frac{\partial \tilde{x}(u-\tau)}{\partial \tau} \times e^{jw(t-u)}E\left[y(t)y^*(u)\right]dtdu + \iint_{-\infty}^{\infty}\tilde{x}^*(t-\tau)\frac{\partial^2 x(u-\tau)}{\partial \tau^2} \times e^{jw(t-u)}E\left[y(t)y^*(u)\right]dtdu\right\}. \tag{21}$$

The correlation of $y(t)$ is,

$$E[y(t)y^*(u)] = E_r\tilde{x}(t-\tau)\tilde{x}^*(u-\tau)e^{jw(t-u)} + N_0\delta(t-u) + N_R\delta(t-u) \tag{22}$$

$$J_{11} = -2K'\left\{\bar{E}_r\left|\int_{-\infty}^{\infty}\frac{\partial \tilde{x}(t-\tau)}{\partial t}\tilde{x}^*(t-\tau)dt\right|^2 + N_0\int_{-\infty}^{\infty}\left|\frac{\partial \tilde{x}(t-\tau)}{\partial t}\right|^2 dt + \mathrm{Re}\left[\bar{E}_r \times \int_{-\infty}^{\infty}|\tilde{x}(t-\tau)|^2 dt \times \int_{-\infty}^{\infty}\frac{\partial^2 \tilde{x}^*(u-\tau)}{\partial \tau^2}\tilde{x}(u-\tau)du\right] + \mathrm{Re}\left[N_0\int_{-\infty}^{\infty}\tilde{x}(t-\tau)\frac{\partial^2 \tilde{x}^*(t-\tau)}{\partial \tau^2}dt\right] + N_r\int_{\infty}^{\infty}\left|\frac{\partial \tilde{x}(t-\tau)}{\partial t}\right|^2 dt + \mathrm{Re}\left[N_r\int_{-\infty}^{\infty}\tilde{x}(t-\tau)\frac{\partial^2 \tilde{x}^*(t-\tau)}{\partial \tau^2}dt\right]\right\} \tag{23}$$

Here 'Re' represents the real part of this signal component. we further simplify the above equation by considering the following:

$$\int_{-\infty}^{\infty}|\tilde{x}(t-\tau)|^2 dt = 1 \tag{24}$$

It is known that the waveform energy does not rely on the delay. So differentiating (24) with respect to τ, then

$$\mathrm{Re}\left\{\int_{-\infty}^{\infty}\left[\frac{\partial \tilde{x}(t-\tau)}{\partial \tau}\tilde{x}^*(t-\tau)\right]dt\right\} = 0 \tag{25}$$

we again differentiate the above equation, then

$$\mathrm{Re}\left\{\int_{-\infty}^{\infty}\left(\frac{\partial^2 \tilde{x}(t-\tau)}{\partial \tau^2}\tilde{x}^*(t-\tau) + \frac{\partial \tilde{x}(t-\tau)}{\partial \tau}\frac{\partial \tilde{x}^*(t-\tau)}{\partial \tau}\right)dt\right\} = 0 \tag{26}$$

Hence,

$$\mathrm{Re}\left[\int_{-\infty}^{\infty}\frac{\partial^2 \tilde{x}^*(t-\tau)}{\partial \tau^2}\tilde{x}(t-\tau)dt\right] = -\int_{-\infty}^{\infty}\left|\frac{\partial \tilde{x}(t-\tau)}{\partial \tau}\right|^2 dt \tag{27}$$

Hence, from (23) second term, fourth term, and fifth term, the sixth term cancels each other. Further based on Parseval's theorem, the first term represents '$\bar{\omega}^2$' and the third term represents '$\overline{\omega^2}$'. With reference to the above results,

$$J_{11} = 2K'\bar{E}_r\left[\overline{\omega^2} - (\bar{\omega})^2\right] \tag{28}$$

In the same way, the remaining elements of the fisher information matrix elements can be evaluated. Moreover, the derivation of J_{12} and J_{21} is identical. Similarly,

$$J_{12} = J_{21} = 2K'\bar{E}_r\left[\bar{\omega}\bar{t} - \bar{\omega}\bar{t}\right] \tag{29}$$

$$J_{22} = 2K'\bar{E}_r\left[\overline{t^2} - (\bar{t})^2\right] \tag{30}$$

Finally, the fisher information matrix for a given received signal is provided by,

$$\mathbf{J} = \frac{2\bar{E}_r}{N_0+N_r}\left(\frac{\bar{E}_r}{\bar{E}_r+N_0+N_r}\right)\begin{bmatrix}\overline{\omega^2}-(\bar{\omega})^2 & \overline{\omega t}-\bar{\omega}\bar{t}\\ \overline{\omega t}-\bar{\omega}\bar{t} & \overline{t^2}-(\bar{t})^2\end{bmatrix} \tag{31}$$

In general, meantime and mean frequency are equivalent to zero. Any time-domain waveform ensures symmetry with respect to the origin by considering the mean as zero. Further, a zero-mean frequency indicates the transmitted waveform envelope has zero carrier frequency. Thus above equation (31) is modified as,

$$\mathbf{J} = \frac{2\bar{E}_r}{N_0+N_r}\left(\frac{\bar{E}_r}{\bar{E}_r+N_0+N_r}\right)\begin{bmatrix}\overline{\omega^2} & \overline{\omega t}\\ \overline{\omega t} & \overline{t^2}\end{bmatrix} \tag{32}$$

Further, the waveform parameter vector's contribution and signal-to-residual noise ratio (γ) can be isolated. Hence, the Fisher information matrix ($\mathbf{J}$) is expressed as,

$$\mathbf{J} = \gamma\, U(\Theta_k) \tag{33}$$

Here $\gamma = \frac{2\bar{E}_r}{N_0+N_r}\left(\frac{\bar{E}_r}{\bar{E}_r+N_0+N_r}\right)$ and $\mathbf{U}(\boldsymbol{\Theta}_\mathbf{k}) = \begin{bmatrix}\overline{\omega^2} & \overline{\omega t}\\ \overline{\omega t} & \overline{t^2}\end{bmatrix}$ with reference to (33), the measurement noise covariance matrix

is modified as,

$$\mathbf{N}(\mathbf{\Theta_k}) = \frac{1}{\gamma}\mathbf{T}U(\Theta_k)^{-1}T^T \tag{34}$$

B. CALCULATION OF $\mathbf{N}(\Theta_k)$ FOR DESIGNATED WAVEFORMS

In this section, we consider several waveforms to evaluate the measurement noise covariance matrix. Further, it is assumed that mean time ($\bar{t}$) and mean frequency ($\bar{\omega}$) are zero for the waveform envelope of the transmitter [42]. As anticipated, $\overline{\omega t} = 0$ for pure amplitude modulated waveforms as it quantifies the amount of frequency modulation in the pulse signal [43].

1) CONTINUOUS WAVE - RECTANGULAR PULSE

Let $\tilde{x}(t)$ be a rectangular pulse waveform and it is provided by,

$$\tilde{x}(t) = \begin{cases} \frac{1}{\sqrt{T}}, & -\frac{\tau}{2} < t < \frac{\tau}{2} \\ 0, & \text{elsewhere .} \end{cases} \tag{35}$$

$$|\tilde{X}(\omega)| = \frac{2}{\sqrt{\tau}\omega}\sin\left(\frac{\omega\tau}{2}\right) \tag{36}$$

$$\overline{\omega^2} = \frac{4\pi B_1}{\tau}, \quad \overline{t^2} = \frac{\tau^2}{12}, \quad \overline{\omega t} = 0 \tag{37}$$

$$\mathbf{N}(\Theta_k) = \begin{bmatrix} \frac{c^2\tau}{16\gamma\pi B_1} & 0 \\ 0 & \frac{3c^2}{\gamma\tau^2\omega_c{}^2} \end{bmatrix} \tag{38}$$

Further, $|\mathbf{N}(\mathbf{\Theta_k})| = \frac{3c^4}{16\gamma^2\pi B_1\tau\omega_c{}^2}$. Here $|[\cdot]|$ represents the determinant of a matrix. It is evident from the expression that, by maintaining a high signal-to-residual noise ratio (γ) value the measurement noise covariance can be reduced.

2) CONTINUOUS WAVE - TRIANGULAR PULSE

An analog triangular pulse waveform is represented as,

$$\tilde{x}(t) = \begin{cases} \sqrt{\frac{3}{2\tau}}\left(1 - \frac{|t|}{\tau}\right) & -\tau < t < \tau \\ 0 \quad \text{otherwise} \end{cases} \tag{39}$$

$$\tilde{X}(\omega) = \sqrt{\frac{3\tau}{2}}\text{sinc}^2\left(\frac{\omega\lambda}{2}\right) \tag{40}$$

$$\overline{\omega^2} = 3/\tau^2, \quad \bar{t^2} = \tau^2/10, \quad \bar{\omega t} = 0 \tag{41}$$

$$\mathbf{N}(\mathbf{\Theta_k}) = \begin{bmatrix} \frac{c^2\tau^2}{12\gamma} & 0 \\ 0 & \frac{5c^2}{2\omega_c^2\tau^2\gamma} \end{bmatrix} \tag{42}$$

Further, $|\mathbf{N}(\mathbf{\Theta_k})| = \frac{5c^4}{24\gamma^2\omega_c{}^2}$. It is evident from the expression that, by maintaining a high signal-to-residual noise ratio (γ) value the measurement noise covariance can be minimized.

3) CONTINUOUS WAVE - GAUSSIAN PULSE

A Gaussian pulse often obeys a handy analytic idealization and it is represented as,

$$\tilde{x}(t) = \left(\frac{1}{\pi\tau^2}\right)^{1/4}\exp\left(\frac{-t^2}{2\tau^2}\right) \tag{43}$$

$$\tilde{X}(\omega) = \left(4\pi\tau^2\right)^{1/4}\exp\left(\frac{-\omega^2\tau^2}{2}\right) \tag{44}$$

$$\overline{\omega^2} = 1/2\tau^2, \quad \overline{t^2} = \tau^2/2, \quad \overline{\omega t} = 0 \tag{45}$$

$$\mathbf{N}(\mathbf{\Theta_k}) = \begin{bmatrix} \frac{c^2\tau^2}{2\gamma} & 0 \\ 0 & \frac{c^2}{2\omega_c^2\tau^2\gamma} \end{bmatrix} \tag{46}$$

Further, $|\mathbf{N}(\mathbf{\Theta_k})| = \frac{c^4}{4\gamma^2\omega_c{}^2}$. It is evident from the expression that, by maintaining a high signal-to-residual noise ratio (γ) value the measurement noise covariance can be reduced. In a nutshell, for the above-selected amplitude-modulated waveforms, the selection of optimized waveform parameter vector (Θ_k) is provided by the following objective function,

$$\begin{aligned} &\underset{\mathbf{\Theta_k}}{\text{minimize}} \; |\mathbf{N}(\mathbf{\Theta}_k)| \\ &\text{subject to} \quad \gamma_{\max} \end{aligned} \tag{47}$$

Here, '$\mathbf{\Theta_k}$' represents the received waveform parameter vector at instant 'k'. Further, the maximized signal-to-residual noise ratio ($\gamma_{\max}$) is the waveform constraint (tunable waveform parameter) in all the designated amplitude-modulated waveforms. In addition, the optimization problem (47) is solved using the *MATLAB* linear programming solver [44]. Hence, by controlling the measurement noise covariance, the radar target tracking performance can be improved in the JRCS.

To perform target state estimation based on uncertain measurements, the determinant or trace of a measurement noise covariance matrix as an objective function is a meaningful optimization approach [45]. Since, the measurement noise covariance matrix ($\mathbf{N}(\mathbf{\Theta_k})$) follows eigenvector matrix decomposition and similarity transformation as in (8) [46], the determinant of a matrix or the trace of a matrix optimization provides the same solution [45]. Therefore, in this investigation $|\mathbf{N}(\mathbf{\Theta_k})|$ is considered and the objective function is evaluated using the determinant approach.

4) LFM-PULSE

A linear frequency-modulated pulse waveform is suitable for pulse compression to achieve high-range resolution. Mathematically, it is given by,

$$\tilde{x}(t) = A_1\cos\left(\pi\frac{B_1}{\tau}t^2\right) \quad -\frac{\tau}{2} \le t \le \frac{\tau}{2} \tag{48}$$

Here, A_1 represents the amplitude of the waveform, B_1 represents the waveform bandwidth and τ indicates the pulse

duration.

$$\tilde{X}(\omega) \approx |\tilde{X}(\omega)| \exp\left(-j\frac{1}{4\pi}\frac{\tau}{B_1}\omega^2\right)\exp\left(j\frac{\pi}{4}\right) \tag{49}$$

Here $|\tilde{X}(\omega)| \approx 1$, $-\pi B_1 \leq \omega \leq \pi B_1$ and for all the remaining ω values $|\tilde{X}(\omega)| = 0$.

Subsequently, $\overline{\omega^2} = \frac{2\pi^3 {B_1}^3}{3}$, $\overline{t^2} = \frac{A_1^2\tau^3}{12}$ and $\overline{\omega t} = \frac{A_1^2\tau^2\pi B_1}{6}$

$$\mathbf{N}(\mathbf{\Theta_k}) = \beta \begin{bmatrix} \frac{3c^2A_1^2\tau^3}{4\gamma} & \frac{-3c^2{A_1}^2\tau^2\pi B_1}{2\omega_c\gamma} \\ \frac{-3c^2{A_1}^2\tau^2\pi B_1}{2\omega_c\gamma} & \frac{6c^2\pi^3{B_1}^3}{\gamma{\omega_c}^2} \end{bmatrix} \tag{50}$$

Where $\beta = \left(\frac{1}{A_1^2B_1^2\tau^2\pi^2(2\tau\pi B_1 - A_1^2\tau^2)}\right)$ and $|\mathbf{N}(\mathbf{\Theta_k})| = \beta^2 \left(\frac{18c^4\pi^3\tau^3{A_1}^2{B_1}^3 - 9c^4\pi^2\tau^4{A_1}^4{B_1}^2}{4\gamma^2{\omega_c}^2}\right)$. It is evident from the expression that, $|\mathbf{N}(\mathbf{\Theta_k})|$ can be reduced by considering optimal signal bandwidth (B_{1opt}) and high signal-to-residual noise ratio (γ) value. Hence the selection of the waveform parameter vector ($\mathbf{\Theta_k}$) is given by the following objective function,

$$\begin{aligned} &\underset{\mathbf{\Theta_k}}{\text{minimize}} \quad |\mathbf{N}(\mathbf{\Theta_k})|, \\ &\text{subject to} \quad \gamma_{\max} \\ &\qquad\qquad B_{\min} < B_{1opt} < B_{\max} \end{aligned} \tag{51}$$

Here '$\mathbf{\Theta_k}$' represents the received waveform parameter vector at time instant 'k'. From (51) the optimal waveform bandwidth (B_{1opt}) is obtained based on the optimization problem defined in [42], using minimum bandwidth ($B_{\min}$), maximum bandwidth ($B_{\max}$) as the constraints of the optimization problem. i.e., $B_{\min} < B_{1opt} < B_{\max}$. In addition, the optimization problem is solved based on the signal-to-residual noise ratio (γ) and bandwidth ($B_{\min}$, $B_{\max}$) as constraints [44]. By tuning the waveform parameters of the LFM-pulse, we can minimize the measurement noise covariance, thereby achieving an enhanced radar target tracking performance in the JRCS.

5) LFM-GAUSSIAN PULSE

Let $\tilde{x}(t)$ be an LFM-Gaussian pulse and it is provided by,

$$\tilde{x}(t) = \left(\frac{1}{\pi\tau^2}\right)^{1/4} \exp\left[-\left(\frac{1}{2\tau^2} - jb\right)t^2\right] \tag{52}$$

$$\tilde{X}(\omega) = \frac{\left(4\pi\tau^2\right)^{1/4}}{\sqrt{1-2jb\tau^2}} \exp\left(\frac{-\omega^2\tau^2}{2\left(1-2jb\tau^2\right)}\right)$$

$$\overline{\omega^2} = \left(1/2\tau^2\right) + 2b^2\tau^2, \quad \overline{t^2} = \tau^2/2, \quad \overline{\omega t} = b\tau^2 \tag{53}$$

$$\mathbf{N}(\mathbf{\Theta_k}) = \begin{bmatrix} \frac{c^2\tau^2}{2\gamma} & \frac{-c^2b\tau^2}{\omega_c\gamma} \\ \frac{-c^2b\tau^2}{\omega_c\gamma} & \frac{c^2}{\omega_c^2\gamma}\left(\frac{1}{2\tau^2} + 2b^2\tau^2\right) \end{bmatrix} \tag{54}$$

Further, $|\mathbf{N}(\mathbf{\Theta_k})| = \frac{c^4}{4{\omega_c}^2\gamma^2}$. It is evident from (54) and $|\mathbf{N}(\mathbf{\Theta_k})|$ that, the measurement noise covariance can be reduced by choosing maximum sweep rate ($b_{\max}$) and maximum signal-to-residual noise ratio ($\gamma_{\max}$) values. Hence the waveform parameter vector ($\mathbf{\Theta_k}$) is selected based on the following optimization problem,

$$\begin{aligned} &\underset{\mathbf{\Theta_k}}{\text{minimize}} \; |\mathbf{N}(\mathbf{\Theta_k})|, \\ &\text{subject to} \quad \gamma_{\max} \\ &\qquad\qquad b_{\max} \end{aligned} \tag{55}$$

Here, the maximized signal-to-residual noise ratio($\gamma_{\max}$) and maximized sweep rate ($b_{\max}$) are the waveform constraints (tunable waveform parameters) of the optimization problem (55). Here, the optimization problem is solved using *MATLAB* linear programming solver [44]. By properly selecting tunable waveform parameters of the LFM-Gaussian pulse, we can minimize the measurement noise covariance and achieve an improved radar target tracking performance.

Constraints are finding a feasible solution from a large set of candidates. In addition, the nature of the optimization problem (convex or non-convex) also depends on the type of constraint (Linear or non-linear). However, in this article, the optimization problems are defined in (47), (51), and (55) for the selection of waveform parameter vector (Θ_k) based on the signal-to-residual-noise ratio (γ) and the bandwidth such that the measurement noise covariance ($\mathbf{N}(\mathbf{\Theta_k})$) is minimum. Further, an algorithm is presented below to solve the aforementioned optimization problems:

According to [9], the vector Θ_k, characterizes the waveform parameters (amplitude, frequency, and sweep rate) of the waveform received at a time instant 'k' and is represented using measurement noise covariance matrix ($\mathbf{N}(\mathbf{\Theta_k})$). Here, for all the amplitude-modulated radar waveforms, the optimization problem is formulated in (47). In (47), the amplitude-modulated radar waveform is constrained by signal-to-residual noise ratio (γ). Further, in (51) the LFM-pulse radar waveform is constrained by waveform signal-to-residual noise ratio (γ) and waveform bandwidth (B). Furthermore, in (55) the LFM-Gaussian pulse radar waveform is constrained by the signal-to-residual-noise ratio (γ) and sweep rate ($b_{\max}$).

Algorithm 1: Procedure to solve the optimization problems using linear programming solver.

Result: Θ_k= The optimal waveform parameter vector
Selection: Choose γ, B_1, and b for the optimal selection of $\mathbf{\Theta_k}$ to minimize $\mathbf{N}(\mathbf{\Theta_k})$
Steps:
1. Define the objective function, and declare the vectors corresponding to the constraints
2. Set upper and lower bounds on the design variables
3. If the constraints are not present then set vector = [ ]
4. Finally the *linprog( )MATLAB* function is used to solve the objective function.

6) NLFM - PULSE

The NLFM-pulse waveform is widely used due to its special characteristics like low side-lobe ratio, and high flexibility [14]. A second-order NLFM pulse with a polynomial phase is represented as,

$$\tilde{x}(t) = e^{i\pi\left(p_1 B^2 t^2 + p_2 B^4 t^4\right)} \quad -\frac{\tau}{2} \le t \le \frac{\tau}{2} \tag{56}$$

Here p_1, p_2 are phase coefficients of the phase polynomial, and B_1 represents the bandwidth. Based on the Principle of Stationary Phase (PSP) approximation, the spectrum of the signal is expressed as,

$$\begin{aligned}\tilde{X}(\omega) &\approx 2\sqrt{\frac{-\pi}{2\Phi''(t_0,\omega)}}e^{-i\frac{\pi}{4}}\tilde{x}(t_0)\,e^{i\Phi(t_0,\omega)} \\ &= 2\sqrt{\frac{-1}{4p_1{B_1}^2 + 24p_2{B_1}^4 t_0^2}}e^{-i\frac{\pi}{4}}e^{i\pi\left(p_1{B_1}^2 t_0^2 + p_2{B_1}^4 t_0^4\right)} \\ &\quad \cdot e^{i\pi\left(p_1{B_1}^2 t_0^2 + p_2{B_1}^4 t_0^4 - 2ft_0\right)}\end{aligned} \tag{57}$$

Here $\Phi''(t,\omega) = \frac{\partial^2\Phi(t,\omega)}{\partial t^2} = \pi(2p_1{B_1}^2 + 12p_2{B_1}^4 t^2)$. Further, $|\tilde{X}(\omega)| \approx 1$, $-\pi B_1 \le \omega \le \pi B_1$ and for all the remaining ω values $|\tilde{X}(\omega)| = 0$.

Subsequently, $\overline{\omega^2} = \frac{8\pi^3{B_1}^3}{3(4p_1{B_1}^2 + 24p_2{B_1}^4 t_0^2)}$, $\overline{t^2} = \frac{\tau^3}{12}$ and $\overline{\omega t} = \frac{\pi p_1 B_1^2 \tau^3}{6} + \frac{\pi p_2 {B_1}^4 \tau^5}{20}$

$$\begin{aligned}\mathbf{N}(\boldsymbol{\Theta}_\mathbf{k}) = \frac{1}{\gamma}\mathbf{T} \\ \times \begin{bmatrix} \frac{\tau^3}{12} & \frac{\pi p_1 B_1^2 \tau^3}{6} + \frac{\pi p_2 {B_1}^4 \tau^5}{20} \\ \frac{\pi p_1 B_1^2 \tau^3}{6} + \frac{\pi p_2 {B_1}^4 \tau^5}{20} & \frac{8\pi^3{B_1}^3}{3(4p_1{B_1}^2 + 24p_2{B_1}^4 t_0^2)} \end{bmatrix} \mathbf{T}^T\end{aligned} \tag{58}$$

Here $\mathbf{T} = \mathrm{diag}(c/2, c/(2\omega_c))$, '$c$' represents the waveform propagation velocity and ω_c is the carrier frequency. In NLFM pulse waveform, phase coefficients (p_1, p_2) and signal-to-residual noise ratio (γ) are the waveform constraints (tunable waveform parameters). Here the optimized phase coefficients (p_1, p_2) are evaluated based on our previous work [14]. From (58), it is evident that the measurement noise covariance can be minimized by optimizing the phase coefficients and maximizing the (γ) value. Further, by minimizing the measurement noise covariance an improved radar target tracking performance can be accomplished in the JRCS.

With reference to Table 1, the measurement noise covariance matrix ($\mathbf{N}(\boldsymbol{\Theta}_\mathbf{k})$) is evaluated for all the designated waveforms. It is noticed that selecting a radar waveform and its tunable parameters plays an important role in minimizing the measurement noise covariance such that efficient target estimation performance can be achieved. From the above analysis, the standard deviation of the range and range rate measurements is calculated for designated waveforms and is listed in Table 2. It is noticed that the NLFM-pulse waveform exhibits the minimum range and range rate measurement errors compared to other waveforms.

TABLE 2. Standard Deviation of Range and Range Rate Measurements for Various Waveforms

Type of waveform	Range standard deviation(σ)	Range rate standard deviation(σ)
Rectangular pulse	8.48 m	7.87 m/s
Triangular pulse	7.62 m	7.61 m/s
Gaussian pulse	5.91 m	7.07 m/s
LFM pulse	6.98 m	6.02 m/s
LFM Gaussian pulse	5.91 m	4.86 m/s
NLFM pulse	5.10 m	3.70 m/s

C. COMPLEXITY OF THE PROPOSED ALGORITHM

In the proposed work, the complexity of the algorithm varies in evaluating the $\mathbf{N}(\boldsymbol{\Theta}_\mathbf{k})$ for various waveforms. Since the evaluation of $\mathbf{N}(\boldsymbol{\Theta}_\mathbf{k})$, depends on the selection of waveform parameters and its optimization problem. In addition, the algorithm's complexity mainly depends on the convergence of the optimization problem. If the waveform and its optimization problem are non-convex, then it will take more time to converge. Hence, the complexity of the proposed algorithm varies by the type of waveform.

IV. TARGET TRACKING

A single radar sensor operating in a co-located configuration produces the measurements pertaining to the target present in the surveillance. These measurements are filtered and estimate the state of interest.

A. MEASUREMENT AND STATE MODEL

The measurement model is given by,

$$z_j(k) = HX(k) + n_j(k) \tag{59}$$

Here $X(k)$ is the state vector at k^{th} time instant, H represents a measurement transition matrix, and $n_j(k)$ represents the measurement noise. The measurement vector is a stacked form of range and range rate, which is represented as $z_k = [r_k \quad \dot{r}_k]^T$, where r and $\dot{r}$ represents the range and range rate respectively. Similarly, the state is given by $X = [r, \dot{r}, \ddot{r}]$. Since the measurement and state are in a linear relation, in (59) the measurement model is represented as a multiplication of state and measurement. The measurement transition matrix can be written as

$$H = \begin{bmatrix} 1 & 0 & 0 \\ 0 & 1 & 0 \end{bmatrix}. \tag{60}$$

Both the noise components present in range and range rate are independent and identically distributed (iid) and follow a Gaussian random process with mean as zero and standard deviation σ_r and $\sigma_{\dot{r}}$ respectively. The waveform parameter vector '$\boldsymbol{\Theta}_\mathbf{k}$' characterizes the received waveform at time instant 'k' and it is incorporated in the measurement noise covariance matrix $\mathbf{N}(\boldsymbol{\Theta}_\mathbf{k}) = \mathbb{E}\{n(k)n(k)'\}$. The target kinematic model is given by

$$X(k+1) = F(k)X(k) + w(k) \tag{61}$$

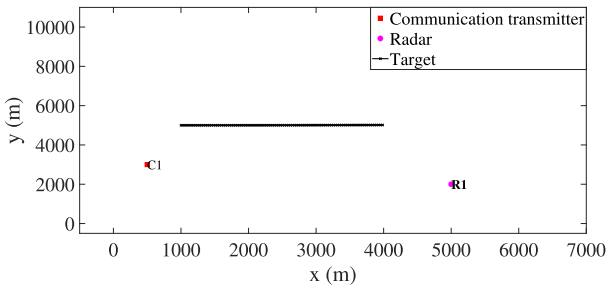

FIGURE 3. Generating a scenario for a single radar-sensor, single communication transmitter

Where '$X(k)$' represents a state vector and '$w(k)$' is a Gaussian distributed white noise vector having zero mean and its covariance matrix is expressed as $Q(k) = \mathbb{E}[w(k)w(k)']$. The process noise vector $w(k)$ is due to the perturbation in r, $\dot{r}$, and $\ddot{r}$ dimensions. Here $F(k)$ denotes the state transition matrix for the constant range rate

$$F(k) = \begin{bmatrix} 1 & t_s & t_s/2 \\ 0 & 1 & t_s \\ 0 & 0 & 1 \end{bmatrix}, \tag{62}$$

Here 't_s' represents the sampling time interval. This measurement generation is carried out under the condition of target detection probability ($p_d = 1$) and probability of false alarm ($p_{fa} = 0$). The target generation is considered to be the CV model rather than the constant turn model. The reason behind this assumption is to illustrate the significance of extracted measurement noise covariance corresponding to the waveforms. In the case of non-linear trajectories and non-linear measurement relationships, the extended Kalman filters and IMM filters are required. It is hard to illustrate the significance of the extracted measurement noise covariance matrix parameter. Hence, the rest of the filtering is carried out using the Kalman filter owing to its optimal behaviour for linearity and Gaussian assumptions.

B. FILTERING

There are three major steps involved in filtering, namely state prediction, calculation of gain, and then state updation. Firstly, the predicted state is expressed as,

$$\hat{X}(k+1 \mid k) = F\hat{X}(k \mid k) \tag{63}$$

subsequently, the predicted covariance is provided by,

$$P(k+1 \mid k) = FP(k \mid k)F' + Q(k) \tag{64}$$

The predicted measurement is expressed as,

$$\hat{r}(k+1) = H\hat{X}(k+1 \mid k) \tag{65}$$

Using the predicted measurement and actual observation, the innovation is calculated as

$$\gamma = z(k+1) - \hat{z}(k+1|k), \tag{66}$$

The gain of Kalman filter K is expressed as,

$$K(k+1) = P(k+1/k)H(k+1)' \tag{67}$$

$$\left[H(k+1)P(k+1/k)H(k+1)' + \mathbf{N}(\mathbf{\Theta_k})\right]^{-1}, \tag{68}$$

Here $\mathbf{N}(\mathbf{\Theta_k})$ represents the measurement noise covariance matrix. Based on the above equations, the updated state is given by,

$$\hat{X}(k+1 \mid k+1) = \hat{X}(k+1 \mid k) + K(k+1)\gamma(k+1) \tag{69}$$

subsequently, the updated covariance is provided by,

$$P(k+1 \mid k+1) = P(k+1 \mid k) - K(k+1)H(k+1)K'(k+1) \tag{70}$$

C. POSTERIOR CRAMER-RAO LOWER BOUND (PCRLB)

In this article, we consider a standard theoretical lower bound posterior Cramer Rao lower bound (PCRLB) [22] to validate the state estimation. Let $X(k+1)$ be the state vector and estimation of the state vector with respect to the measurement set $z_{1:k+1}$ is denoted as $\hat{X}(k+1)$. According to [47], the PCRLB on the covariance matrix $P(k+1)$ is evaluated by taking the inverse of the Fisher Information Matrix (FIM) ($J(k+1)$).

$$P(k+1) \triangleq \mathbb{E}\Big[\Big(\hat{X}(k+1) - X(k+1)\Big)\Big(\hat{X}(k+1) - X(k+1)\Big)'\Big] \geq \mathbf{J(k+1)^{-1}}, \tag{71}$$

Where,

$$\mathbf{J(k+1)} = \left[F(k)^{-1}\right]^T J(k)F(k)^{-1} + Q(k)^{-1} + H(k)^T\mathbf{N}(\mathbf{\Theta_{k+1}})^{-1}H(k) \tag{72}$$

Based on the measurement noise covariance matrix formula in (34), $\mathbf{N}(\mathbf{\Theta_{k+1}})$ is expressed as,

$$\mathbf{N}(\mathbf{\Theta_{k+1}}) = \frac{1}{\gamma}\mathbf{TU}(\mathbf{\Theta_{k+1}})^{-1}\mathbf{T}^T \tag{73}$$

V. RESULTS AND ANALYSIS

The results and analysis discussed in this section witness the significance of optimum waveform selection for enhancing tracking performance. A single in-band communication transmitter and a radar sensor are assumed to elucidate the uncertainty of radar target tracking in the existence of in-band communication residual interference.

A. SCENARIO GENERATION

In the simulation scenario, we considered that a JRC receiver is assumed to be stationary and has a maximum detectable range of $R_{\max} = 50$ Km. From Fig. 3, it is considered that the radar sensor is located at $[5000, 2000]'$ and an in-band communication transmitter is located at $[500, 2500]'$. Here the radar is mono-static; hence the JRC receiver node is also

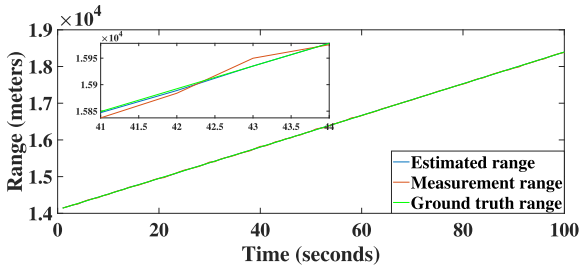

(a) Range measurement for a rectangular pulse waveform

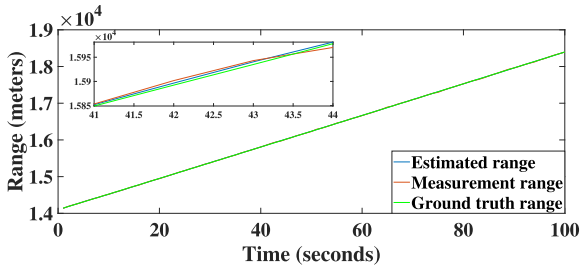

(b) Range measurement for an NLFM waveform

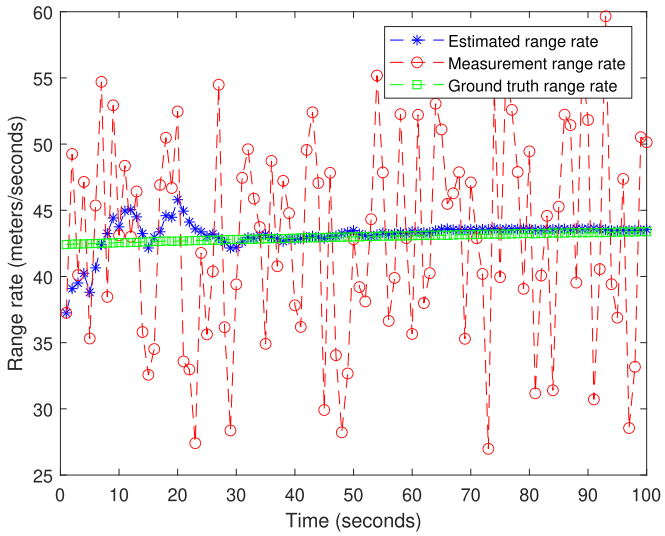

(c) Range rate measurement for a rectangular pulse waveform

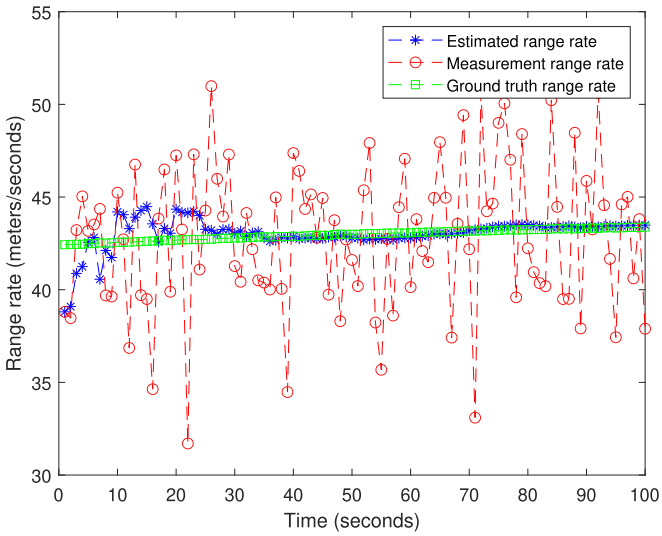

(d) Range rate measurement for an NLFM waveform

FIGURE 4. Comparison of range and range rate for rectangular and NLFM waveforms.

at the radar position. Within the surveillance, a target is at [10000, 10000] and moving with 40 m/s and 20 m/s along x and y directions, respectively. In addition to that, throughout the simulation scenario, the target is assumed to follow a Constant Velocity (CV) motion model. The perturbation of the target is modeled as process noise, and it adheres to an additive white Gaussian noise distribution. The noise components corresponding to position are $\mathcal{N}(0, 0.05^2)$, where, $\mathcal{N}(\mu, \sigma^2)$ is a Gaussian pdf having mean (μ) and variance (σ^2). Similarly, the noise component in velocity is taken as $\mathcal{N}(0, 0.02^2)$. The total simulation time is 100 s with a sampling interval of 1 s. The radar provides the radar data (here data means the measurements of the radar) in range and range-rate. The radar sensor receives the range and range rate measurements corresponding to the radar waveform of operation at the JRC node.

B. TRACK FILTERING

The Kalman Filter(KF) is applied to estimate the range and range rate values at various instants of time. For the track initialization, a one-point initialization approach [48] is considered, and the maximum velocity is tuned to $V_{\max} = 40$ m/s. A Constant Velocity (CV) motion model is utilized in the prediction steps. The process noise covariance is chosen as

$$Q = \begin{bmatrix} \mathcal{N}(0, 0.05^2) \\ \mathcal{N}(0, 0.02^2) \\ \mathcal{N}(0, 0.05^2) \\ \mathcal{N}(0, 0.02^2) \end{bmatrix}. \tag{74}$$

The optimized measurement noise is used for the calculation of innovation covariance.

As an illustration, for example, two different waveforms and the same ground truth are considered to compare the importance of computing the measurement noise and the superiority of the waveform. Fig. 4 illustrates the visualization of the ground truth range and range rate measurements, the observed measurements, and the estimated state. Fig. 4(a) and Fig. 4(b) show the estimated range and acquired range measurement in comparison to ground truth for rectangular-pulse and NLFM-pulse waveforms, respectively. Since the range is in the order of 10^4 m, it is hard to visualize. Further, Fig. 4(c) and Fig. 4(d) show the estimated range rate and acquired range rate measurement in comparison to ground truth for rectangular-pulse and NLFM-pulse waveforms, respectively. Here, we can see that the ground truth range rate is around

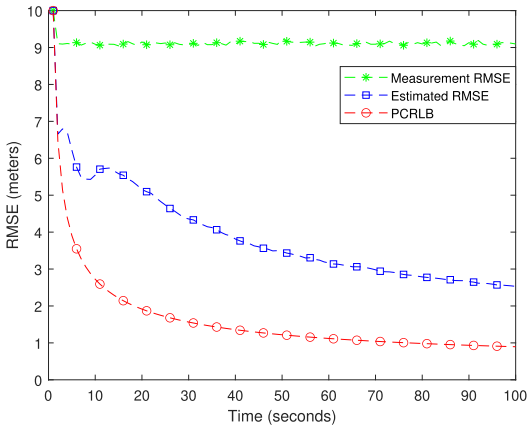

(a) Rectangular pulse waveform

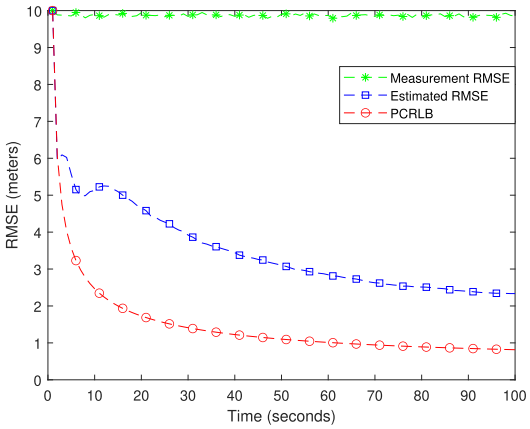

(b) Triangular pulse waveform

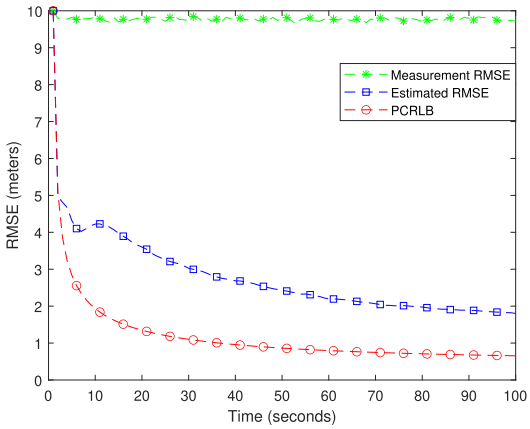

(c) Gaussian pulse waveform

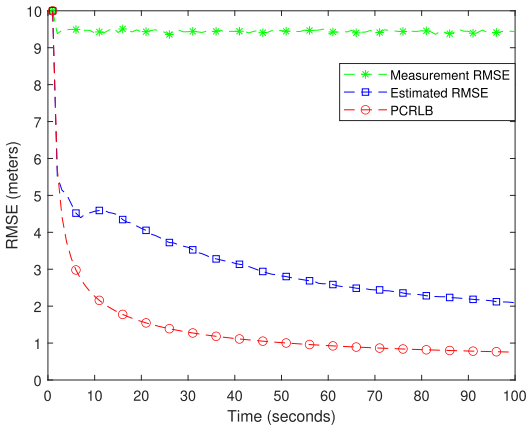

(d) LFM pulse waveform

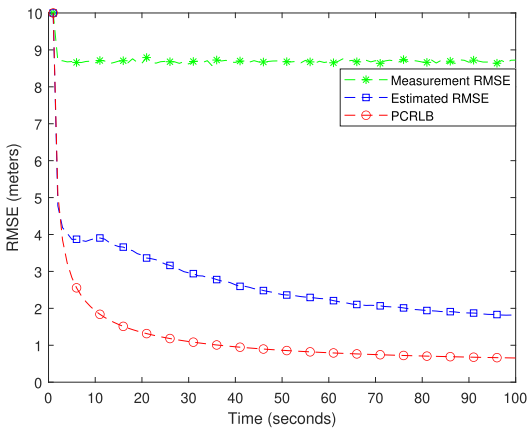

(e) LFM Gaussian pulse waveform

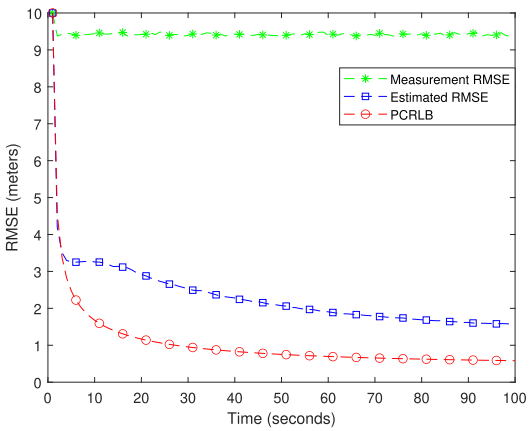

(f) NLFM pulse waveform

FIGURE 5. Analyzing range measurement error for the selected radar waveforms.

43 m/s, whereas the acquired range rate measurements fluctuate around the ground truth range rate with their standard deviations of the waveform. It is worth noting that the estimated range rate fluctuates initially due to the initialization problem. After that, it saturates over time. During the estimation process, the filter is fine-tuned using the range and range rate covariances acquired from Table 2 for both rectangular pulse and NLFM-pulse waveforms. Further, it is also evident

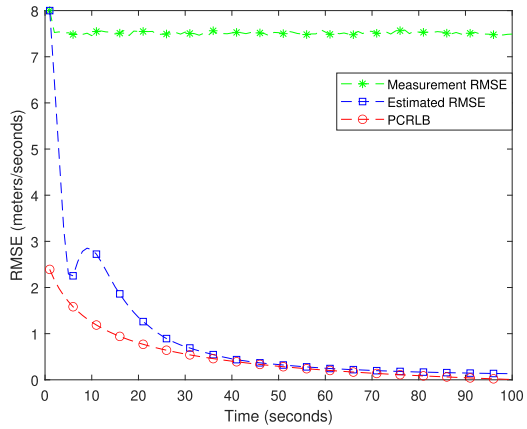

(a) Rectangular pulse waveform

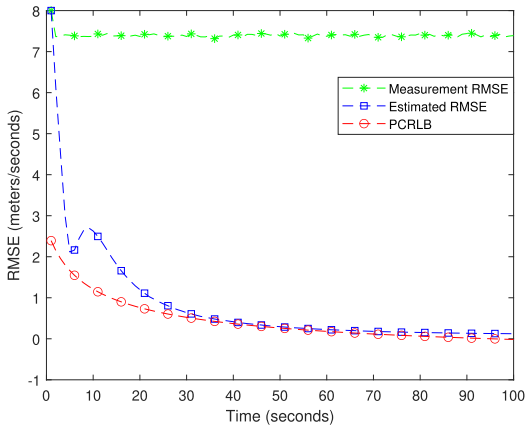

(b) Triangular pulse waveform

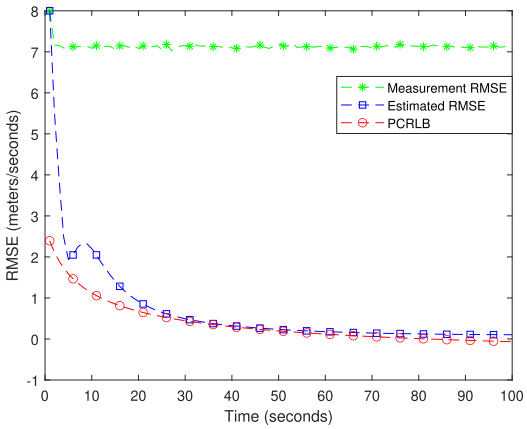

(c) Gaussian pulse waveform

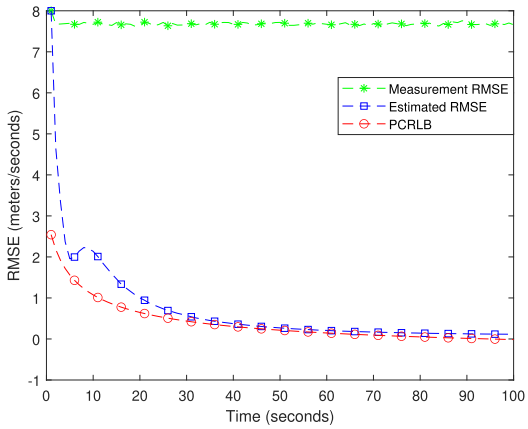

(d) LFM pulse waveform

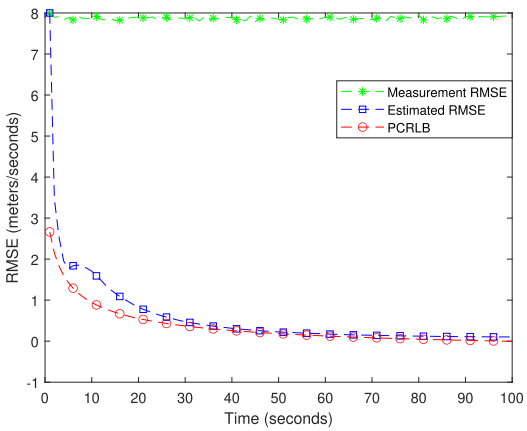

(e) LFM Gaussian pulse waveform

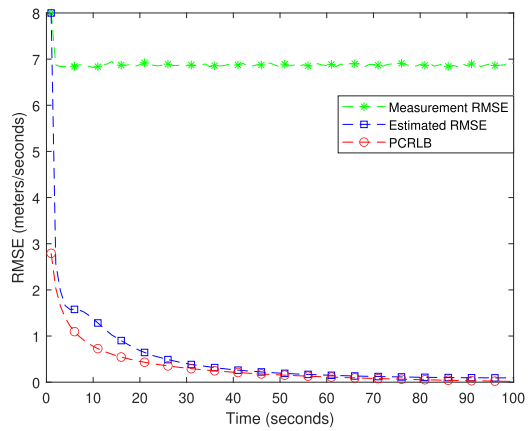

(f) NLFM pulse waveform

FIGURE 6. Analyzing range rate measurement error for the selected radar waveforms.

that the optimized NLFM-pulse waveform exhibits fewer fluctuations in the range and range rate estimations. However, by visualization, it is hard to conclude the superiority of the waveforms. Therefore, one can achieve a more comprehensive performance analysis by estimating the Root Mean Square Error (RMSE) for the range and range rate measurements.

The RMSE of range measurement is plotted in Fig. 5(a)–(f) for the selected waveforms. It is perceived that the estimated RMSE is compared with both the measurement RMSE

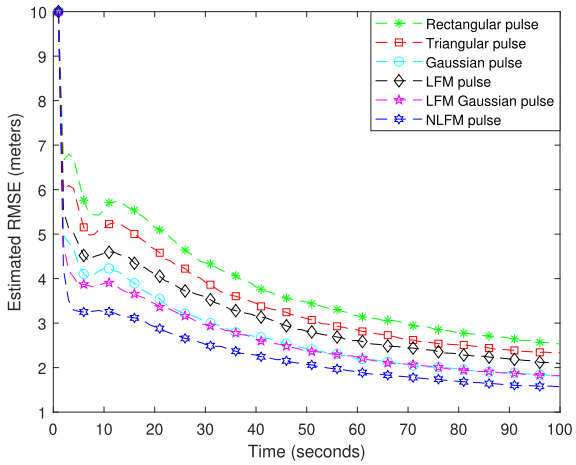

FIGURE 7. Analyzing estimated range measurement error for various designated waveforms

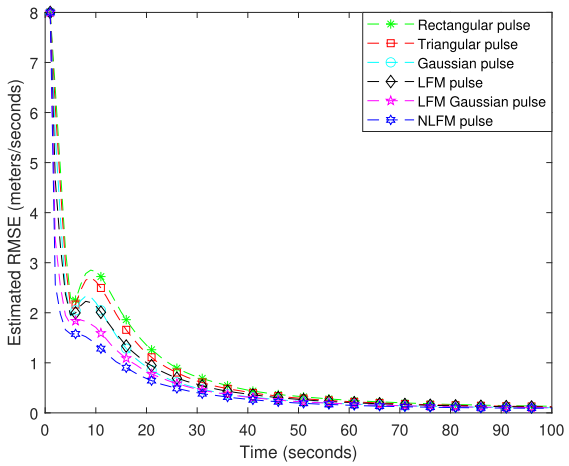

FIGURE 8. Analyzing estimated range rate measurement error for various designated waveforms

(before filtering) and PCRLB for all the selected waveforms. Besides, it is also noticed that the estimated RMSE (range measurement error) values are gradually decreasing by the time scan for all the designated waveforms. In addition, the estimated RMSE values are within the PCRLB limit for all the waveforms in the given time duration. Among all the waveforms, the optimized NLFM-pulse waveform outperforms the remaining waveforms in terms of deviation between estimated RMSE and PCRLB. That is, estimated RMSE values of the NLFM-pulse waveform are approaching the minimum error variance. We also observed that frequency-modulated waveforms (LFM-pulse, LFM-Gaussian pulse, and NLFM-pulse) outperform the amplitude-only modulated waveforms (rectangular pulse, triangular pulse, and Gaussian pulse) in terms of range error.

In Fig. 6(a)–(f), the estimated range rate error values are compared with both the measurement RMSE (before filtering) and PCRLB from a range rate perspective for all the selected waveforms. Further, it is noticed that the estimated RMSE (range rate measurement error) values are gradually decreasing in accordance with the time scan (as shown in Fig. 6(a)–(f)). Furthermore, it is also perceived that the estimated range rate RMSE values are within the PCRLB limit at all time instants for all the designated waveforms. Among all the selected waveforms, the optimized NLFM-pulse waveform outperforms the remaining waveforms in terms of deviation between the estimated RMSE and the PCRLB. That is, range rate RMSE values of the NLFM-pulse waveform are approaching minimum error variance. We also observed that the frequency-modulated waveforms (LFM-pulse, LFM-Gaussian pulse, and NLFM-pulse) provide improved performance compared to amplitude-only modulated waveforms(rectangular pulse, triangular pulse, and Gaussian pulse) in terms of range rate RMSE. The estimated range RMSE of various waveforms is plotted in Fig. 7. It is evident from the plot that the estimated range RMSE values for all the waveforms are gradually decreasing with the increasing number of time scans. Further, the range RMSE of the NLFM-pulse waveform yields improved performance compared to the remaining waveforms. Furthermore, the range RMSE values of the rectangular pulse waveform are high (which is undesirable) compared to other designated waveforms. Fig. 8 shows the range rate RMSE of various selected waveforms in a joint radar-communication system. It is noticed from the plot that the range rate RMSE for all the waveforms is gradually decreasing in accordance with the increasing number of time scans. Additionally, the range rate RMSE of the NLFM-pulse waveform provides superior performance compared to the remaining waveforms. In addition, the range rate RMSE of the rectangular pulse waveform provides poor performance compared to other designated waveforms.

Here, we quantified the Monte-Carlo-based simulation results against the PCRLB. It is noticed that the RMSE is decreasing over time and coming very near the theoretical PCRLB value. This intuitively shows that the measured covariance from the waveform characteristics is an optimal approach compared to tuning the measurement noise covariance. In addition, the PCRLB value and RMSE value for the NLFM waveform are low, which gives an understanding that the filtering/tracking accuracy is high.

Figs. 9 and 10 analyze the impact of the communication residual component on the accuracy of estimating the radar target's state in a JRCS. These figures compare the proposed approach (including the communication residual component) with the traditional approach (excluding the communication residual component). Fig. 9 compares the estimated range measurement error of various selected radar waveforms between the traditional and proposed methods. In addition, the effect of the communication residual component is evident from all the chosen radar waveforms. As time increases, the estimated range measurement error gradually decreases for all the designated radar waveforms. Among all the radar waveforms, the NLFM radar waveform exhibits better performance, i.e., the effect of the communication residual

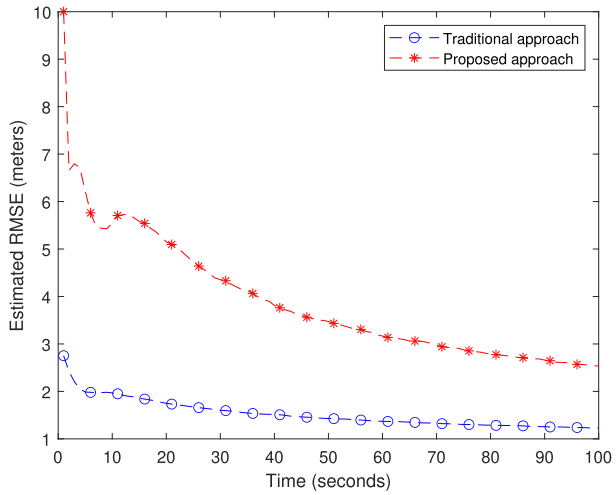

(a) Rectangular pulse waveform

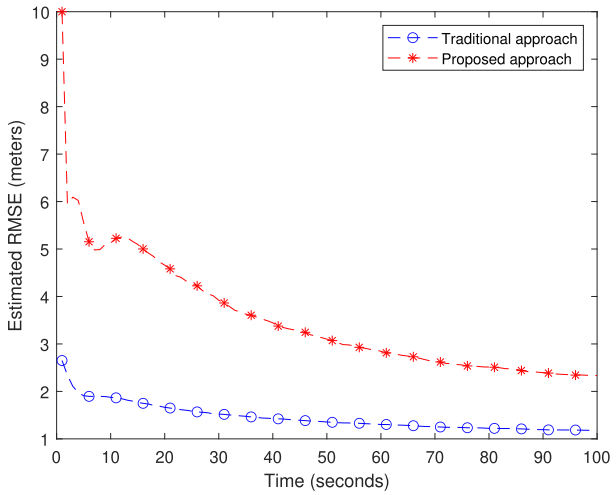

(b) Triangular pulse waveform

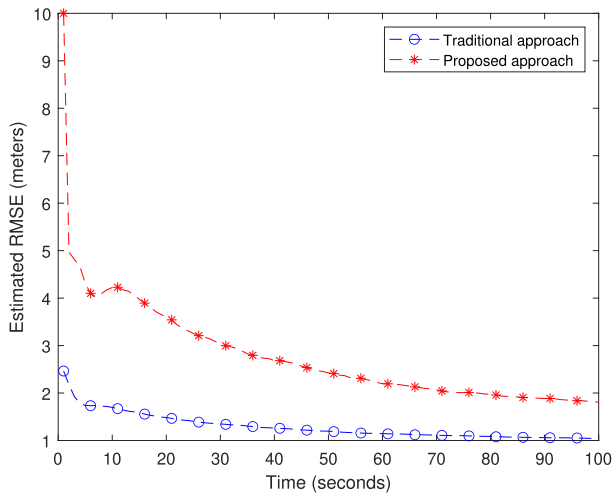

(c) Gaussian pulse waveform

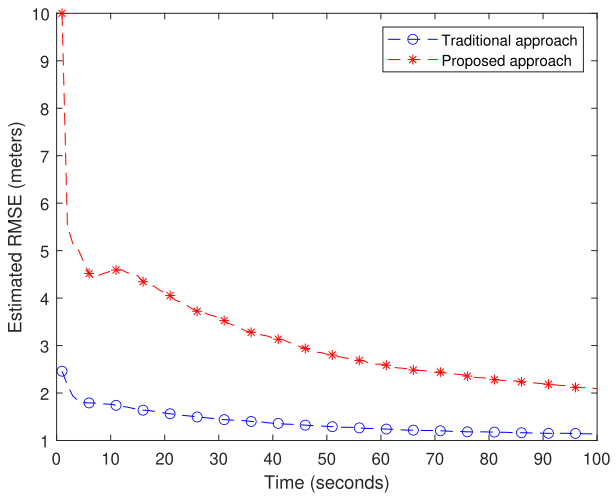

(d) LFM pulse waveform

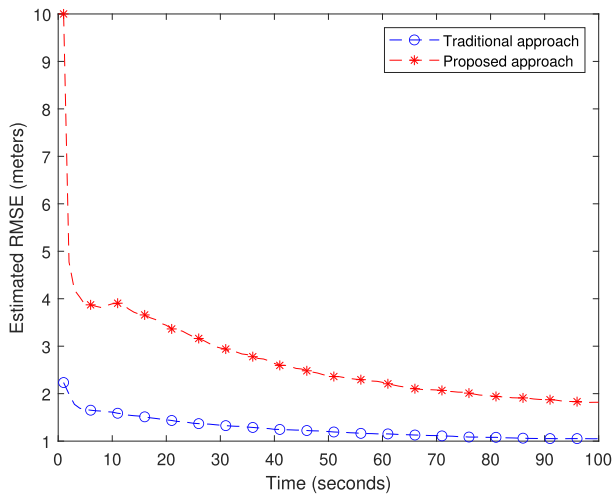

(e) LFM Gaussian pulse waveform

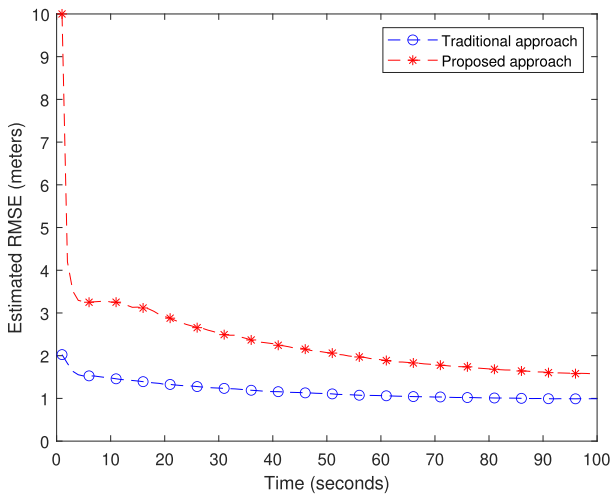

(f) NLFM pulse waveform

FIGURE 9. **Comparing estimated range measurement error of the traditional and proposed approaches for the selected radar waveforms.**

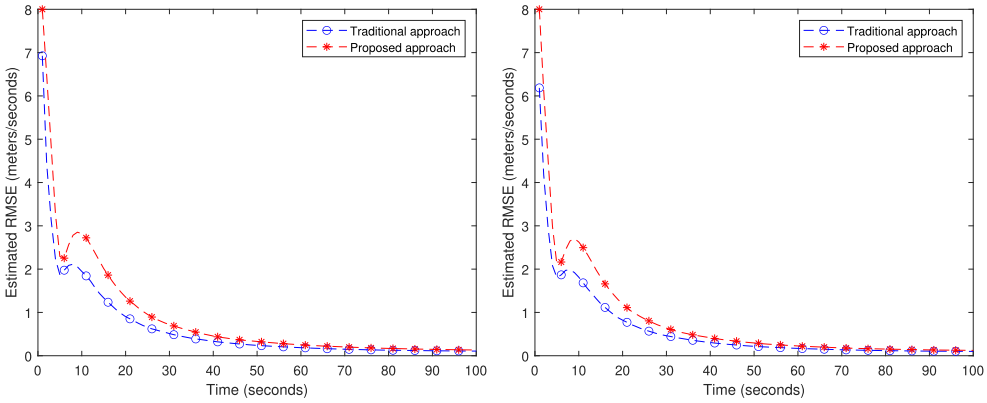

(a) Rectangular pulse waveform

(b) Triangular pulse waveform

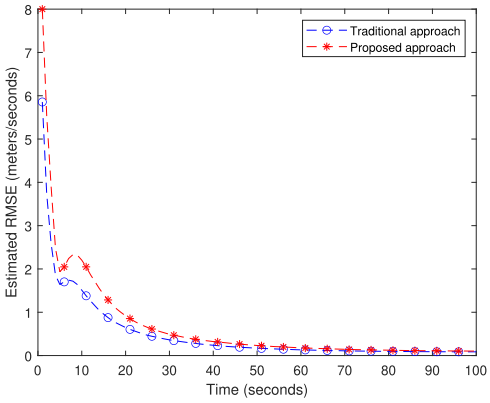

(c) Gaussian pulse waveform

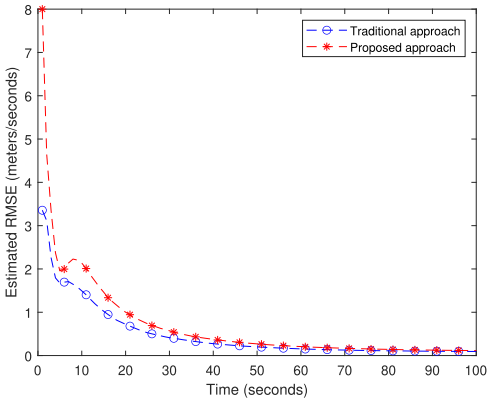

(d) LFM pulse waveform

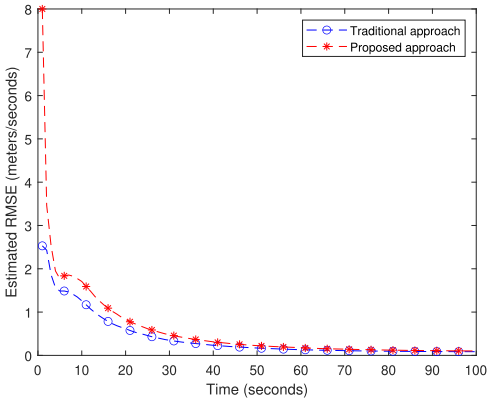

(e) LFM Gaussian pulse waveform

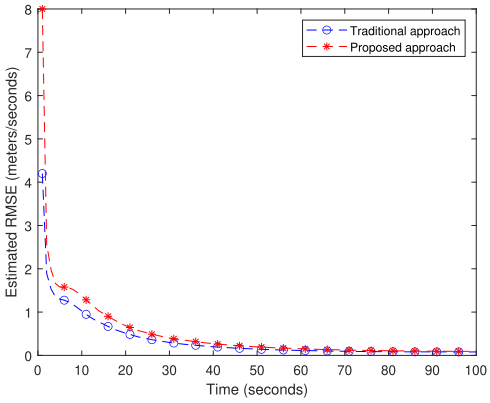

(f) NLFM pulse waveform

FIGURE 10. Comparing estimated range rate measurement error of the traditional and proposed approaches for the selected radar waveforms.

component is minimal compared to the rest of the selected radar waveforms. In addition, the NLFM radar waveform achieved a minimum range error deviation of 0.5 m in a joint radar-communication system.

Furthermore, Fig. 10 compares the proposed and traditional approaches in terms of estimated range rate measurement error for various designated radar waveforms. We observe the impact of the communication residual component across all radar waveforms. Out of the chosen radar waveforms, the NLFM radar waveform effectively mitigates the effect of the communication residual component, resulting in improved performance when estimating radar range rate. Moreover, the NLFM radar waveform completely overcomes the effect of the communication residual component at the higher time values, i.e., 50 s − 100 s.

VI. CONCLUSION

A novel measurement model is introduced with a communication residual component to investigate the performance of a radar system in the JRCS framework. The proposed technique derived a Fisher Information Matrix (FIM), which helped characterize a radar sensor for the selected waveforms

in the spectrum-sharing scenario. Further, the Kalman filter is deployed to estimate the target kinematics regarding range and range rate. Among all the designated waveforms, it is apparent that the NLFM-pulse waveform provided superior performance in range and range rate RMSE values. Because the optimized NLFM-pulse waveform exhibits reduced side-lobes in the matched filter output and achieves maximum signal-to-residual noise ratio even without a side-lobe filter. It is noticed that the frequency-modulated waveforms (LFM-pulse, LFM-Gaussian pulse, and NLFM-pulse) accomplished improved performance compared to the amplitude-modulated waveforms (rectangular pulse, triangular pulse, Gaussian-pulse) in terms of range and range rate RMSE. Hence, selecting waveform and its tunable parameters like optimal signal bandwidth, sweep rate, and signal-to-residual noise ratio is prominent in achieving improved target tracking performance in the JRCS configuration.

This research investigation is carried out with a single target without clutter and Electronic Countermeasures (ECM). Hence, with this novel measurement model, one can carry out future research in the direction of single-target and multiple-target tracking in clutter and/or ECM. Further, another future research direction would be incorporating clutter and/or intentional interference to the measurement model and the communication residual component to perform comprehensive research.

APPENDIX

A. RELATION BETWEEN LIKELIHOOD FUNCTION AND LIKELIHOOD RATIO

The complex envelope of the received waveform on the two hypotheses are

$$y(t)=\sqrt{E_r}e^{j\Phi}\tilde{x}(t-\tau)e^{j\omega t}+n(t)+s_{com}^{resi}(t),\ 0\le t\le T:H_1,$$
$$y(t)=n(t)+s_{com}^{resi}(t),\quad 0\le t\le T:H_0, \tag{75}$$

In the complex case, we correlate $y(t)$ with $\tilde{x}^*(t-\tau)$, and it is defined as a likelihood function. Hence, it is expressed as,

$$L(\tau,\omega)=\int_{\infty}^{\infty}y(t)\tilde{x}^*(t-\tau)\exp^{-j\omega t}\,dt \tag{76}$$

According to [42], the likelihood ratio is defined as,

$$\Lambda(\tau,\omega)=\frac{p_{L(\tau,\omega)|H_1}((\tau,\omega)|H_1)}{p_{L(\tau,\omega)|H_0}((\tau,\omega)|H_0)}$$
$$=\frac{(1/\pi(\bar{E}_r+N_0+N_r))\exp(-(L(\tau,\omega))^2/(\bar{E}_r+N_0+N_r))}{(1/\pi(N_0+N_r))\exp(-(L(\tau,\omega))^2/(N_0+N_r))} \tag{77}$$

Here $\bar{E}_r$ represents the average received signal energy, N_0 denotes the thermal noise power, and N_r signifies the residual noise power. The above expression is simplified, and the result is obtained as,

$$\Lambda(\tau,\omega)=\frac{N_0+N_r}{\bar{E}_r+N_0+N_r}$$
$$.\exp\left(\left(L\left(\tau,\omega\right)\right)^2.\left(\frac{\bar{E}_r}{(\bar{E}_r+N_0+N_r)(N_0+N_r)}\right)\right. \tag{78}$$

By applying natural logarithms on both sides of the equation, then the result becomes

$$\ln\Lambda(\tau,\omega)=\frac{1}{N_0+N_r}\frac{\bar{E}_r}{\bar{E}_r+N_0+N_r}\left\{|L(\tau,\omega)|^2\right\} \tag{79}$$

REFERENCES

[1] H. Griffiths et al., "Radar spectrum engineering and management: Technical and regulatory issues," *Proc. IEEE*, vol. 103, no. 1, pp. 85–102, Jan. 2015.

[2] P.C. of Advisors on Science and Technology, "Realizing the full potential of government-held spectrum to spur economic growth," Jul. 2012. [Online]. Available: https://obamawhitehouse.archives.gov/sites/default/files/microsites/ostp/pcast/spectrumreport

[3] A. R. Chiriyath, B. Paul, and D. W. Bliss, "Radar-communications convergence: Coexistence, cooperation, and co-design," *IEEE Trans. Cogn. Commun. Netw.*, vol. 3, no. 1, pp. 1–12, Mar. 2017.

[4] G. Srinath, B. Pardhasaradhi, A. C. Mahipathi, P. K. H, P. Srihari, and L. R. Cenkeramaddi, "Performance analysis of spectrum sharing radar in multipath environment," *IEEE Open J. Commun. Soc.*, vol. 4, pp. 922–935, 2023.

[5] F. Liu, C. Masouros, A. P. Petropulu, H. Griffiths, and L. Hanzo, "Joint radar and communication design: Applications, state-of-the-art, and the road ahead," *IEEE Trans. Commun.*, vol. 68, no. 6, pp. 3834–3862, Jun. 2020.

[6] D. W. Bliss, "Cooperative radar and communications signaling: The estimation and information theory odd couple," in *Proc. IEEE Radar Conf.*, 2014, pp. 0050–0055.

[7] J. A. Zhang et al., "An overview of signal processing techniques for joint communication and radar sensing," *IEEE J. Sel. Topics Signal Process.*, vol. 15, no. 6, pp. 1295–1315, Nov. 2021.

[8] C. Sturm and W. Wiesbeck, "Waveform design and signal processing aspects for fusion of wireless communications and radar sensing," *Proc. IEEE*, vol. 99, no. 7, pp. 1236–1259, Jul. 2011.

[9] D. J. Kershaw and R. J. Evans, "Optimal waveform selection for tracking systems," *IEEE Trans. Inf. Theory*, vol. 40, no. 5, pp. 1536–1550, Sep. 1994.

[10] R. Niu, P. Willett, and Y. Bar-Shalom, "Tracking considerations in selection of radar waveform for range and range-rate measurements," *IEEE Trans. Aerosp. Electron. Syst.*, vol. 38, no. 2, pp. 467–487, Apr. 2002.

[11] R. M. Mealey, "A method for calculating error probabilities in a radar communication system," *IEEE Trans. Space Electron. Telemetry*, vol. 9, no. 2, pp. 37–42, Jun. 1963.

[12] A. Hassanien, M. G. Amin, Y. D. Zhang, and B. Himed, "A dual-function MIMO radar-communications system using PSK modulation," in *Proc. IEEE 24th Eur. Signal Process. Conf.*, 2016, pp. 1613–1617.

[13] A. R. Chiriyath, S. Ragi, H. D. Mittelmann, and D. W. Bliss, "Novel radar waveform optimization for a cooperative radar-communications system," *IEEE Trans. Aerosp. Electron. Syst.*, vol. 55, no. 3, pp. 1160–1173, Jun. 2019.

[14] A. C. Mahipathi, S. Gunnery, S. Pathipati, J. D'Souza, and P. Jena, "Nonlinear frequency modulated waveform optimization for a cooperative radar-communication system," in *Proc. IEEE Int. Conf. Electron. Comput. Commun. Technol.*, 2021, pp. 1–6.

[15] J. A. Mahal, A. Khawar, A. Abdelhadi, and T. C. Clancy, "Spectral coexistence of MIMO radar and MIMO cellular system," *IEEE Trans. Aerosp. Electron. Syst.*, vol. 53, no. 2, pp. 655–668, Apr. 2017.

[16] E. Yousif, F. Khan, T. Ratnarajah, and M. Sellathurai, "On the spectral coexistence of colocated MIMO radars and wireless communications systems," in *Proc. IEEE 17th Int. Workshop Signal Process. Adv. Wireless Commun.*, 2016, pp. 1–5.

[17] M. Bică and V. Koivunen, "Radar waveform optimization for target parameter estimation in cooperative radar-communications systems," *IEEE Trans. Aerosp. Electron. Syst.*, vol. 55, no. 5, pp. 2314–2326, Oct. 2019.

[18] D. P. Zilz and M. R. Bell, "Statistical modeling of wireless communications interference and its effects on adaptive-threshold radar detection," *IEEE Trans. Aerosp. Electron. Syst.*, vol. 54, no. 2, pp. 890–911, Apr. 2018.

[19] G. Srinath, H. P. Kumar, P. Srihari, R. Tharmarasa, and T. Kirubarajan, "Coherent radar target detection with in-band cyclostationary wireless interference," *IEEE Access*, vol. 10, pp. 11173–11190, 2022.

[20] J. A. S. M. A. Richards and W. A. H. Raleigh, *Principles of Modern Radar:basic Principles, Ser*. 1st ed. Edison, New Jersey, USA: SciTech Publishing, 2010.
[21] X. R. L. Y. Bar-Shalom and T. Kirubarajan, *Estimation With Applications to Tracking and Navigation: Theory Algorithms and Software*. Hoboken, NJ, USA: Wiley, 2004.
[22] P. K. W. Y. Bar-Shalom and X. Tian, *Tracking Data Fusion, Ser*. 1st ed. Storrs, Connecticut, USA: YBS Publishing, 2010, vol. 11.
[23] A. Sinha, Z. Ding, T. Kirubarajan, and M. Farooq, "Track quality based multitarget tracking approach for global nearest-neighbor association," *IEEE Trans. Aerosp. Electron. Syst.*, vol. 48, no. 2, pp. 1179–1191, Apr. 2012.
[24] Y. Bar-Shalom, F. Daum, and J. Huang, "The probabilistic data association filter," *IEEE Control Syst. Mag.*, vol. 29, no. 6, pp. 82–100, Dec. 2009.
[25] X. Jiang, K. Harishan, R. Tharmarasa, T. Kirubarajan, and T. Thayaparan, "Integrated track initialization and maintenance in heavy clutter using probabilistic data association," *Signal Process.*, vol. 94, pp. 241–250, 2014. [Online]. Available: https://www.sciencedirect.com/science/article/pii/S0165168413002442
[26] Y. Bar-Shalom and T. E. Fortmann, *Tracking and Data Association*. Cambridge, MA, USA: Academic Press, 1988.
[27] D. Kershaw and R. Evans, "Waveform selective probabilistic data association," *IEEE Trans. Aerosp. Electron. Syst.*, vol. 33, no. 4, pp. 1180–1188, Oct. 1997.
[28] S. P. Sira, A. Papandreou-Suppappola, and D. Morrell, "Advances in waveform-agile sensing for tracking," *Synth. Lectures Algorithms Softw. Eng.*, vol. 1, no. 1, pp. 1–83, 2008. [Online]. Available: https://doi.org/10.2200/S00168ED1V01Y200812ASE002
[29] S. P. Sira, A. Papandreou-Suppappola, and D. Morrell, "Dynamic configuration of time-varying waveforms for agile sensing and tracking in clutter," *IEEE Trans. Signal Process.*, vol. 55, no. 7, pp. 3207–3217, Jul. 2007.
[30] C. Rago, P. Willett, and Y. Bar-Shalom, "Detection-tracking performance with combined waveforms," *IEEE Trans. Aerosp. Electron. Syst.*, vol. 34, no. 2, pp. 612–624, Apr. 1998.
[31] S. Sira, D. Morrell, and A. Papandreou-Suppappola, "Waveform design and scheduling for agile sensors for target tracking," in *Proc. IEEE Conf. Rec. 38th Asilomar Conf. Signals Syst. Comput.*, 2004, pp. 820–824.
[32] W. Blair, G. Watson, T. Kirubarajan, and Y. Bar-Shalom, "Benchmark for radar allocation and tracking in ECM," *IEEE Trans. Aerosp. Electron. Syst.*, vol. 34, no. 4, pp. 1097–1114, Oct. 1998.
[33] S. P. Sira, Y. Li, A. Papandreou-Suppappola, D. Morrell, D. Cochran, and M. Rangaswamy, "Waveform-agile sensing for tracking," *IEEE Signal Process. Mag.*, vol. 26, no. 1, pp. 53–64, Jan. 2009.
[34] G. S. Satapathi and S. Pathipati, "Waveform agile sensing approach for tracking benchmark in the presence of ECM using immpdaf," *Radioengineering*, vol. 26, no. 1, pp. 227–239, 2017.
[35] S. Gunnery, P. Bethi, P. H. Kumar, and S. Pathipati, "Target estimation performance improvement in cooperative radar and communication system spectrum sharing," in *Proc. IEEE 12th Int. Conf. Comput. Commun. Netw. Technol.*, 2021, pp. 1–6.
[36] G. Srinath, B. Pardhasaradhi, P. Kumar H., and P. Srihari, "Tracking of radar targets with in-band wireless communication interference in radcomm spectrum sharing," *IEEE Access*, vol. 10, pp. 31955–31969, 2022.
[37] A. Zhang, M. L. Rahman, X. Huang, Y. J. Guo, S. Chen, and R. W. Heath, "Perceptive mobile networks: Cellular networks with radio vision via joint communication and radar sensing," *IEEE Veh. Technol. Mag.*, vol. 16, no. 2, pp. 20–30, Jun. 2021.
[38] R. S. Thoma et al., "Cooperative passive coherent location: A promising 5G service to support road safety," *IEEE Commun. Mag.*, vol. 57, no. 9, pp. 86–92, Sep. 2019.
[39] A. Aubry, V. Carotenuto, A. De Maio, A. Farina, and L. Pallotta, "Optimization theory-based radar waveform design for spectrally dense environments," *IEEE Aerosp. Electron. Syst. Mag.*, vol. 31, no. 12, pp. 14–25, Dec. 2016.
[40] A. R. Chiriyath, B. Paul, and D. W. Bliss, "Joint radar-communications information bounds with clutter: The phase noise menace," in *Proc. IEEE Radar Conf. (RadarConf)*, 2016, pp. 1–6.
[41] J. Xie, T. Hong, T. Laing, and C. Kang, "On normality assumption in residual simulation for probabilistic load forecasting," *IEEE Trans. Smart Grid*, vol. 8, no. 3, pp. 1046–1053, May 2017.
[42] H. L. V., *Trees, Detection, Estimation and Modulation Theory*, Hoboken, NJ, USA: Wiley, 1971.
[43] C. W. Helstrom, *Statistical Theory of Signal Detection, Ser*, 2nd ed., New York, USA, 1966.
[44] P. Venkataraman, *Applied Optimization With MATLAB Programming*. Hoboken, NJ, USA: Wiley, 2009.
[45] M. Reinhardt, B. Noack, and U. D. Hanebeck, "Closed-form optimization of covariance intersection for low-dimensional matrices," in *Proc. IEEE 15th Int. Conf. Inf. Fusion*, 2012, pp. 1891–1896.
[46] R. Horn and C. Johnson, *Matrix Analysis*, Cambridge, U.K.: Cambridge Univ. Press, 2005.
[47] P. Tichavsky, C. Muravchik, and A. Nehorai, "Posterior Cramer-Rao bounds for discrete-time nonlinear filtering," *IEEE Trans. Signal Process.*, vol. 46, no. 5, pp. 1386–1396, May 1998.
[48] D. Musicki and T. L. Song, "Track initialization: Prior target velocity and acceleration moments," *IEEE Trans. Aerosp. Electron. Syst.*, vol. 49, no. 1, pp. 665–670, Jan. 2013.

ASHOKA CHAKRAVARTHI MAHIPATHI (Member, IEEE) received the B.Tech. degree in electronics and communication engineering from Jawaharlal Nehru Technological University, Kakinada (JNTU-K), Andhra Pradesh, India, in 2009, and the M.Tech. degree in telecommunications from the National Institute of Technology Durgapur (NIT-D), West Bengal, India, in 2012. Since 2018, he has been working toward the Ph.D. degree (full-time) in electronics and communication engineering with the National Institute of Technology Karnataka (NIT-K), Surathkal, Mangalore, India. He was an Assistant Professor with the Department of Electronics and Communication Engineering, K L University, Vijayawada, Andhra Pradesh, India, till 2018. His research interests include the area of cognitive radio, RF communications and sensing, optimum radar waveform design, and target tracking.

BETHI PARDHASARADHI (Member, IEEE) received the B.Tech. degree in electronics and communication engineering from Jawaharlal Nehru Technological University Kakinada, Kakinada, India, in 2014, the M.Tech. degree in VLSI design from the ABV-Indian Institute of Information Technology and Management, Gwalior, India, in 2016, and the Ph.D. degree in electronics and communication engineering from the National Institute of Technology Karnataka, India, in 2022. Moreover, he was a Visiting Ph.D. Scholar for 16 months at Estimation Tracking and Fusion (ETF) Laboratory, McMaster University, Hamilton, ON, Canada, under the supervision of Prof. T. Kirubarajan, during 2018–2019. In addition, he was also a Visiting Researcher as part of Indo-Norwegian Collaboration to Autonomous and Cyber-Physical Systems (ACPS) Research Group, Department of Information and Communication Technology (ICT), University of Agder, Grimstad, Norway, under the supervision of Prof. Linga Reddy Cenkeramaddi, during 2021–2022. He is currently a technical Specialist with the ADAS Department in Continental Autonomous Mobility India Pvt. Ltd., India. His research interests include intentional interference to autonomous sensors, target tracking, and information fusion. He was the recipient of Sir C. V. Raman Award from the Institution of Engineering and Technology (IET) for Outstanding Academics and Research. Received Best Ph.D Thesis 2022 in Graduate Thesis Evaluation in 7- minutes (GraTE-7) from IEEE ComSoc Graduate Congress. In addition, he was also the recipient of the IEEE ITS Research Excellence Award In 2023 from IEEE information theory society (ITS) Bangalore chapter. Moreover, receipt of Protsahan award from IEEE ComSoc and best papers recognition from IEEE conferences.

SRINATH GUNNERY (Member, IEEE) received the B.Tech. degree in electronics and communication engineering from Jawaharlal Nehru Technological University, Anantapur, India, in 2013, and the M.Tech. degree in digital communication from ABV-IIITM, Gwalior, India, in 2016. He is currently working toward the Ph.D. degree in electronics and communication engineering with the National Institute of Technology Karnataka Surathkal, Mangalore, India. From 2018 to 2019, he was a Visiting Ph.D. Student with the Estimation, Tracking, and Fusion Research Laboratory, McMaster University, Hamilton, ON, Canada. His research interests include cognitive radio, radar signal processing, radar and communication system spectrum sharing, and target tracking.

PATHIPATI SRIHARI (Senior member, IEEE) received the B.Tech. degree in electronics and communication engineering from Sri Venkateswara University, Tirupati, India, and the master's degree in communications engineering and signal processing from the University of Plymouth, England, U.K., and the Ph.D. degree from Andhra University, Visakhapatnam, India, in the field of radar signal processing in 2012. He is currently an Assistant Professor with the National Institute of Technology Karnataka, Surathkal, India. He was a Visiting Assistant Professor with McMaster University, Hamilton, ON, Canada in 2014. His research interests include radar target tracking, radar waveform design, and efficient DSP algorithms for radar applications. Dr. Srihari was the recipient of the 2010 IEEE Asia Pacific Outstanding Branch Counselor Award. He is a Senior Member of ACM. He is a Fellow of IETE and a member of IEICE, Japan. He received a Young Scientist Award from the Department of Science and Technology (DST), New Delhi to carry out a sponsored research project entitled Development of efficient target tracking algorithms in the presence of ECM.

JOHN D'SOUZA (Member, IEEE) received the Ph.D. degree in electronics and electrical communication engineering in 1998 from the Indian Institute of Technology Kharagpur, Kharagpur, India. He joined the National Institute of Technology Surathkal, India, as a Faculty Member where he is currently a Professor. His research focuses on error control coding and modulation.

PARAMANANDA JENA (Member, IEEE) received the B.E. degree in electronics and telecommunication engineering from the Veer Surendra Sai University of Technology (VSSUT), Odisha, India, in 1998, and the M.E. degree in microelectronics systems from the Indian Institute of Science, Bangalore, Bangalore, India, in 2005. He is currently a Scientist with the Electronic and Radar Development Establishment, DRDO, Bangalore. His research interests include radar signal processing, waveform design, MIMO radar, and FMCW radar. He has successfully designed FPGA-based signal processors for portable radars and mmWave Collision Avoidance Radar. As a Project Director, he has successfully completed the project Coastal Surveillance Radar (CSR). He is currently the Project Director of the Navigation Radar for the Integrated Combat Suite and System Engineer of the FMCW radar for the Active Protection System.